(Midterm Scientific Report)

Molecular line shape studies for atmospheric remote sensing

Nguyen Thi Huyen Trang, PhD student

Hanoi, December 17, 2020

Supervisor: Dr. Ha Tran, LISA, CNRS, Université Paris Est Créteil, France

Co-Supervisor: Dr. Ngo Ngoc Hoa, Hanoi University of Education, Vietnam

Contents

I. Introduction

The evolution of the chemical composition of the Earth's atmosphere caused by human activities is a very complex problem. In recent years, significant impacts of climate change have been observed. Understanding of the global warming due to anthropogenic emissions is now a major scientific task. It is now established that climate change is due to emission of greenhouse gases and that the chemical composition of the atmosphere is a main factor which affects the Earth's climate [14].

Optical techniques associated with molecular spectroscopy are among the most effective methods in studying the Earth's atmosphere like those of other planets. Comparisons between the measured and calculated spectra enable to retrieve information about the absorbing species present in the atmosphere. For this, a theoretical model is used to describe the spectral profile of the molecular absorption transition. So far, in most available studies, the Voigt profile (Vp) [61] is widely-used to model the spectral shape of isolated lines (i.e. lines not affected by collisional line-mixing). The Vp is a convolution a Gaussian and a Lorentzian profiles taking into account, respectively, two broadening mechanisms: the first resulted from the thermal agility of the molecules (the Doppler broadening) and the second, induced by intermolecular collisions (the Lorentzian broadening)[37]. The Vp can be written in term of the complex probability function for [45] which many effective computer algorithms for its calculation have been proposed [17, 30, 31, 39, 41, 56]. Based on this profile, the spectroscopic parameters (line intensities, positions, pressure broadenings and shiftings ...) in wide spectral ranges for different molecules are now well known and listed in the various spectroscopic databases such as HITRAN [59, 60] or GEISA [53].

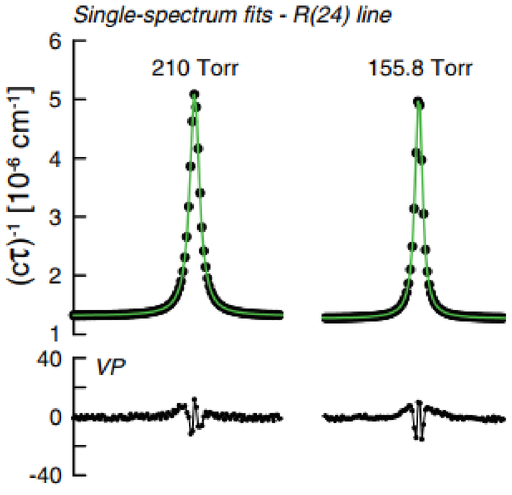

Figure 1a. Measurement spectra of CO_2 in air and the fit residuals by using Single spectrum fits for the *R*(24) transitions for Voigt profile [96]

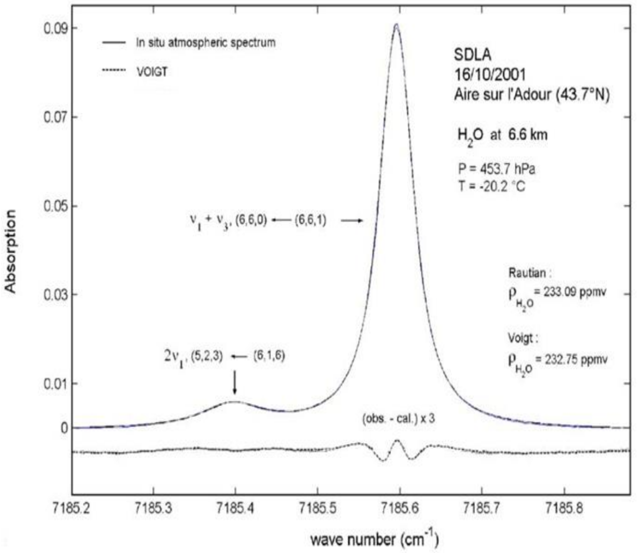

Figure 1b. An in situ absorption spectrum of tropospheric H_2O measured by SDLA and the difference between the measured and calculated spectrum using the Vp.

The accuracy of the calculation of the absorption of solar radiation by atmospheric gases, or of their emission depends on the quality of the line parameters available in these databases. It is therefore necessary to determine with precision line parameters of the molecules of interest. An overall review results provided by different studies [4, 6, 10-21] show that there are significant differences. As for the used spectral profile, it has been shown that the Vp leads to significant difference with the measured spectra [10-13, 46-51, 96]. These differences are generally much greater than the uncertainty of laboratory measurements (Figure 1a) [96] and clearly above the uncertainty of certain remote sensing experiments (Figure 1b) [19]. More reliable approaches beyond the Vp are therefore essential to better meet the expectations of applications.

In fact, the Vp does not take into account two effects which can affect the spectral shape: (i) The velocity changes induced by intermolecular collisions, leading to the so-called Dicke narrowing effect [55] and (ii) the speed dependences of the collisional broadening and shifting [15, 16]. The former is generally modeled using the soft collision model (Galatry profile, Gp [5]) or the hard collision model (Rautian profile, Rp [49, 63]), in which velocity changes are characterized by the frequency of velocity changing collisions (often obtained as an empirical parameter). For the speed dependences of collisional broadening and shifting, a quadratic dependence in absolute speed [15, 16] or a power law in relative velocity (also called a hypergeometric law, [27, 54]) is often used. For each of these approaches, other empirical parameters are then added to describe the speed dependences of collisional parameters. However, experimental results showed limitations of the Rp, Gp and Speed dependence Voigt profile (SDVp) in describing the molecular absorption spectra [20]. Indeed, in the binary collisions regime [43], collisional parameters must linearly depend on the gas pressure. However, it is shown that that the frequency of velocity changing collision (e.g. Fig. 2a) [20] or the speed dependent coefficients of the collisional parameters (e.g. Figure 2b) [51] are non linear with pressure for Rp or SDVp.

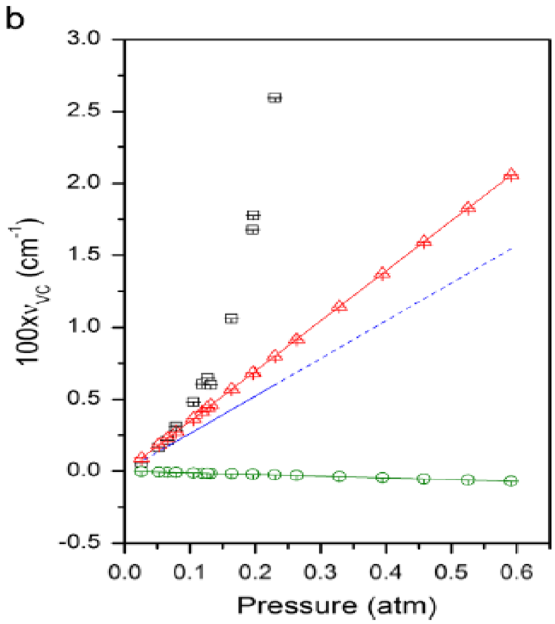

Fig. 2a. Pressure dependence of the Dicke narrowing parameter for the R(20) line of CO_2, obtained from line by line fitting procedure of measured spectra (black squares) using the HC model.

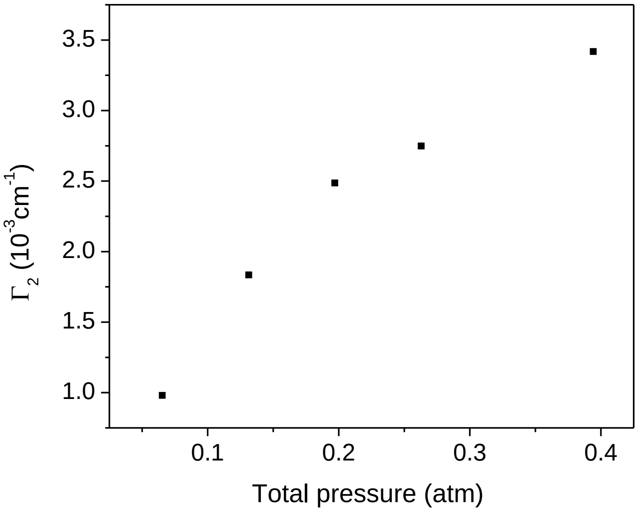

Fig. 2b. Air pressure dependence of the speed dependence parameter Γ_2 for the (606 ← 505) transition of water vapor obtained with the SDVp from line by line fitting procedure of measured spectra.

In 2013, a model that enables a very accurate description of the shapes of absorption lines was proposed (i.e. The Hartmann-Tran profile, HTp, [25,36, 47-51]) for high resolution spectroscopy. This model takes into account several refined processes contributing to the line shape: the Dicke narrowing effect, speed dependences of collisional parameters and the correlation between velocity and rotational-states changes collisions. Comparisons with laboratory spectra have shown that the HTp enables a description of observed line shapes with an accuracy of a few 0.1%. This model was then recommended by the International Union of Pure and Applied Chemistry (IUPAC), as the reference one to be used in spectroscopic and remote sensing studies. Before the HTp can be used for remote sensing, spectroscopic database must be completed with the relevant parameters. Even when limited to key species and regions (*eg* those retained for the remote sensing of greenhouse gases) this is a huge task which cannot be fulfilled rapidly by new laboratory measurements only. The latter are not only difficult to perform with a sufficient accuracy but also lengthy and costly since spectra must be recorded and analyzed for many lines in broad pressure ranges.

This thesis is devoted to accurate predictions of molecular line shapes for atmospheric pressure and temperature conditions for several greenhouse gases such as CO_2, N_2O, CH_3Cl and H_2O. Based on the simultaneous use of first principle calculations and a limited number of measurements together with results of direct predictions by requantized molecular dynamics simulations (rCMDS), this work also focus on the strategy to generate parameters of the HTp for high precision remote sensing.

II. Requantized Classical molecular dynamics simulation for CO_2-N_2/O_2/air; N_2O and analysis procedure

In this part of the thesis, by using rCMDS, one can simulate the time evolution of a very large number of molecules from an intermolecular potential. The auto-correlation function of the dipole moment, responsible for the optical transition can thus be calculated. The Fourier-Laplace transform of this auto-correlation function directly yields the corresponding absorption spectrum. This method was applied to predict lineshape parameters for N_2/O_2/air-broadened CO_2 lines. The rCMDS-calculated spectra of CO_2 in N_2/O_2 were fitted with the speed dependent Nelkin–Ghatak (sdNG) profile in order to retrieve the collisional line broadening coefficient, its speed dependence, the Dicke narrowing and the first order line-mixing parameters. The predicted parameters were then compared with those determined from high quality measurements [69] showing very good agreement, even for the high-order line shape parameters [70]. rCMDS are thus a complementary tool for line-shape studies provided that an accurate intermolecular potential is available. Furthermore, the calculations were performed relatively easily for various temperature conditions, which is not always possible for laboratory measurements. It was demonstrated in a series of papers that rCMDS are capable to reproduce various collisional effects affecting the absorption spectrum of different molecular systems [69–75].

1. Re-quantized classical molecular dynamics simulations

CMDSs were used to perform for the CO_2–N_2 and CO_2–O_2 system using equations described in [82]. All the molecules are considered as rigid rotors.

- **The used intermolecular potential**

  A site-site functional form with Coulombic and atom-atom contributions was used to describe the interaction potential between CO_2 and N_2/O_2 molecules. For this, the molecular geometries and the charges and sites were taken from [73] and [74] for CO_2 and N_2/O_2, respectively. The atom-atom contribution was calculated as a 12-6 Lennard-Jones potential whose parameters were deduced using usual combination laws [83] and parameters for CO_2– CO_2 [74] and N_2–N_2 [73]; O_2– O_2 [73] interactions. The latter were successfully used to predict non-Voigt effects on the line shapes of pure CO_2 [71] and H2O–N_2 [85]; O_2 in air (e.g. [89]). Note that all the effects of vibrational motion were disregarded in the calculations.

- **Temperature and pressure range**

  Calculations were made for the various temperatures of 200 K, 250 K, 296 K at 1 atm for CO_2–N_2 and 200 K, 250 K, 296 K and 350 K for CO_2–O_2 mixtures with 50% of CO_2

- **Facilities**

  Using the IBM Blue Gene/P computer of the *Institut du Dévéloppement et des Ressources en Informatique Scientifique*, the facilities of the faculty of physics at Hanoi National University of Education.

- **Re-quantized classical molecular dynamics simulations**

  Since only CO_2– N_2/O_2 interactions were taken into account, this is equivalent to a mixture of CO_2 infinitely diluted in 0.5 atm of N2 [84]/O_2. For each temperature, a total number of about 3-6 × 10^8 molecules were considered. With a large number of molecules were considered in this type of calculation, a high signal-to-noise ratio of the calculated spectra can be obtained. The molecules were treated in parallel in more than thirty thousand boxes, each containing 20 000 molecules. The molecules were initialized in the boxes as follows: For each molecule, the center-of mass position was randomly chosen with the constraint that molecules should be separated from each other by distances of at least 9 Å. This ensures that no situation involving pairs of unphysically strongly interacting molecules is generated. This condition thus imposes the use of a temporization time in the calculations, which is about 20 ps. Translational and angular speeds verifying the Maxwell-Boltzmann distribution were initialized. Random center-of-mass velocity vector and molecular axis orientation were attributed. The parameters (center-of-mass position, velocity, angular momentum, and molecular orientation) describing the classical state of each molecule were then computed for each time step (up to 900 ps). A requantization procedure, as done in [72] for pure CO2, was applied to the classical rotation of the molecules. Specifically, for a molecule of rotational angular momentum ω, we find the (even) integer J for which $\hbar J/I$, where I is the moment of inertia and is the closest to ω. This corresponds to matching the classical rotational frequency with the quantum position of the P branch lines. Once J is found, ω is requantized by applying the change $\omega = \hbar J/I$, while its orientation is kept unchanged. This P branch requantization implies that the calculated R branch spectrum will be the exact symmetric of the P branch. The auto-correlation function of the dipole moment, assumed along the molecular axis (as the case for the asymmetric stretching absorption bands of CO_2, for instance), was then calculated during the rCMDS. The Doppler effect associated with the translational motion was taken into account in this auto correlation function [72]. For each temperature, eight values of the Doppler width Γ_D (e.g., ranging from 0.002 cm-1 to 0.3 cm-1 at room temperature) were used in the calculations. This provided a large set of values of the ratio Γ_L/Γ_D (e.g., from about 0.08 to 13, at room temperature, Γ_L being the Lorentz width), covering a range from the near purely Doppler to collision-dominant regimes. Note that since all the effects of vibrational motion were disregarded in our rCMDS, this corresponds to eight calculations at eight values of pressure with a unique Doppler width. Finally, the normalized absorption coefficient was obtained as the Fourier-Laplace transform of the auto correlation function of the dipole moment. The spectra were thus calculated without the use of any adjustable parameter. Note that our rCMDSs do not take into account the dephasing of the dipole, which is associated with the fact that the effects of intermolecular interactions for molecules in the upper and lower states of the optical transitions are different. Consequently, the calculated spectra do not show any pressure shift.

The results obtained for CO_2/N_2 and those for CO_2/O_2 will be used to deduce the air-broadened CO_2 line-shape parameters and their temperature dependences.

2. Analysis procedure

Spectra calculated by rCMDS for each temperature were fit with were fit with the speed-dependent Nelkin– Ghatak (sdNG) profile including the first-order line mixing [75]. Within this approach, the absorption coefficient versus wavenumber σ (cm-1) is expressed as [67,76]

$$\alpha(\sigma) \approx \frac{S}{\pi}[\mathrm{Re}\{I^{HT}(\sigma)\} + Y\,\mathrm{Im}\{I^{HT}(\sigma)\}]. \tag{1}$$

In Eq. (1), $Y = P\zeta$ is the first-order line-mixing parameter, where ζ is the pressure-normalized coefficient, which accounts for the coupling between the considered line and other lines. S is the line area. The area-normalized line shape, $I^{HT}(\sigma)$, is, in general, a function of eight parameters, [67,76] i.e.,

$$I^{HT}(\sigma) = f(\sigma - \sigma_0, \mathit{\Gamma}_D, \mathit{\Gamma}_0, \mathit{\Gamma}_2, \mathit{\Delta}_0, \mathit{\Delta}_2, \nu_{vc}, \eta) \tag{2}$$

with σ_0 being the unperturbed position of the line. The HT model takes into account four main processes affecting the shape of an isolated line in the binary-collision regime [76,90] The first one is the Doppler broadening, taken into account through the Doppler width $\mathit{\Gamma}_D$. The second effect is the collision-induced velocity changes (VC) (Dicke narrowing), which are described through the hard-collision model [71,86] in terms of the rate of velocity-changing collisions ν_{VC} (or the Dicke narrowing frequency). This model also takes into account the speed dependences of the collisional half-width $\Gamma(v)$ and shift $\Delta(v)$, modeled by the quadratic law [87 ,91], given by $\mathit{\Gamma}(v) + i\mathit{\Delta}(v) = \mathit{\Gamma}_0 + i\mathit{\Delta}_0 + (\mathit{\Gamma}_2 + i\mathit{\Delta}_2)[(v/\tilde{v})^2 - 3/2]$ in which $\tilde{v} = \sqrt{2k_BT/m}$ is the most probable speed for an absorbing molecule of mass m. Finally, the temporal correlation between velocity-changing and internal-state-changing collisions is accounted for through the correlation parameter η. The line parameters of the HT profile vary simply with the total pressure P: σ_0, and η are constant while ν_{vc}, Γ_0, Γ_2, Δ_0 and Δ_2 are proportional to P (with the corresponding pressure-normalized coefficients: $\gamma_0 = \Gamma_0/P$, $\gamma_2 = \Gamma_2/P$, $\beta = \nu_{vc}/P$, $\delta_0 = \Delta_0/P$ and $\delta_2 = \Delta_2/P$).

In this work, we used a (multi-fitting) procedure in which the spectra of the same line, calculated for various Doppler width values, were simultaneously adjusted. In the fits, the Doppler widths were fixed to values used in the simulations. For each line, the area S, the position σ_0, and a linear base line were adjusted individually, while the line-shape parameters were constrained to be the same for all spectra. The pressure-shifting coefficients δ_0 and δ_2 were fixed to zero since no pressure shift was taken into account in our CMDS. Several tests showed that we cannot retrieve all the remaining parameters of the HT profile. This is probably due to the limited signal-to-noise ratio of the rCMDS-calculated spectra (i.e., from 500 to 5000, depending on the line and on the considered Doppler width). We therefore chose to fix the correlation parameter to zero ($\eta = 0$), and the HT profile thus corresponds to the sdNG (speed dependence Nelkin–Ghatak) [88] limit. Note that this approximation can be safely used for systems for which the frequency of velocity-changing collisions (characterized by the Dicke narrowing parameter) is much smaller than that of the internal-state changing collisions (represented by the line-broadening coefficient). For each line, the line broadening coefficient $\gamma0$, its speed dependence component $\gamma2$, the Dicke narrowing parameter β, and the first-order line-mixing coefficient ζ were retrieved for each temperature. Their temperature dependences were then represented, as also done in the experiment [40] by the usual power law

$$A(T) = A(T_0)(\frac{T_0}{T})^n \qquad (3)$$

with T_0 = 296K – the reference temperature, and $A(T)$ is either γ_0, γ_2, β or ζ and n the temperature dependence exponent. From the values of $A(T)$ obtained at 200 K; 250K and 296K (350K for O_2), the temperature exponent n_A was obtained for each line.

All the simulations and calculations have been done for CO_2 and N_2O deluted in N_2, O_2 and air with various conditions in temperature and pressure as shown in Table 1.

	Temperature ranges	**Pressure**	**Analysis method** Multi-fitting using various models:	**Available parameters**
CO_2-N_2	200, 250, 296K	1 atm with 50% of CO_2	- Voigt profiles - speed-dependent Voigt (no Dicke narrowing effect) - Nelkin–Ghatak (no speed dependence effect): NG	- Line-shape parameter: γ_0, γ_2, β, ξ - Temperature dependence paramteters
CO_2-O_2	200, 250, 296, 350K			
CO_2-air	200, 250, 296K			

			- speed dependent Nelkin–Ghatak: sdNG	
N$_2$O-air	200, 250, 296K	1 atm with 50% of N$_2$O	- quadratic speed-dependent Voigt + first order line mixing - Voigt profiles - speed-dependent Voigt (no Dicke narrowing effect) - speed dependent Nelkin–Ghatak: sdNG	

Table 1: Information of molecular systems have been consisdered

3. Results and discussions

3.1 rCMDS-calculated spectra

The examples of the spectra of some P lines, calculated by rCMDS at various T, and for various Doppler widths are shown in Fig. 3 (CO_2 in N_2), Fig. 4 (CO_2 in O_2), together with the residuals obtained from their multi-fits with sdNG and some simplified models (the speed-dependent Voigt-sdV (no Dicke narrowing effect), the Nelkin–Ghatak-NG (no speed dependence effect) and the widely used Voigt-V profiles). For all the used line profiles, line-mixing effect was taken into account. These show that the sdNG profile leads to very good fits (within 0.1%) of the rCMDS-calculated spectra, the remaining residuals are mostly due to numerical noises of the calculations and not to the used line shape. For comparison, fit residuals obtained with the Voigt profile are also presented where large signatures (up to 2-3%) can be observed.

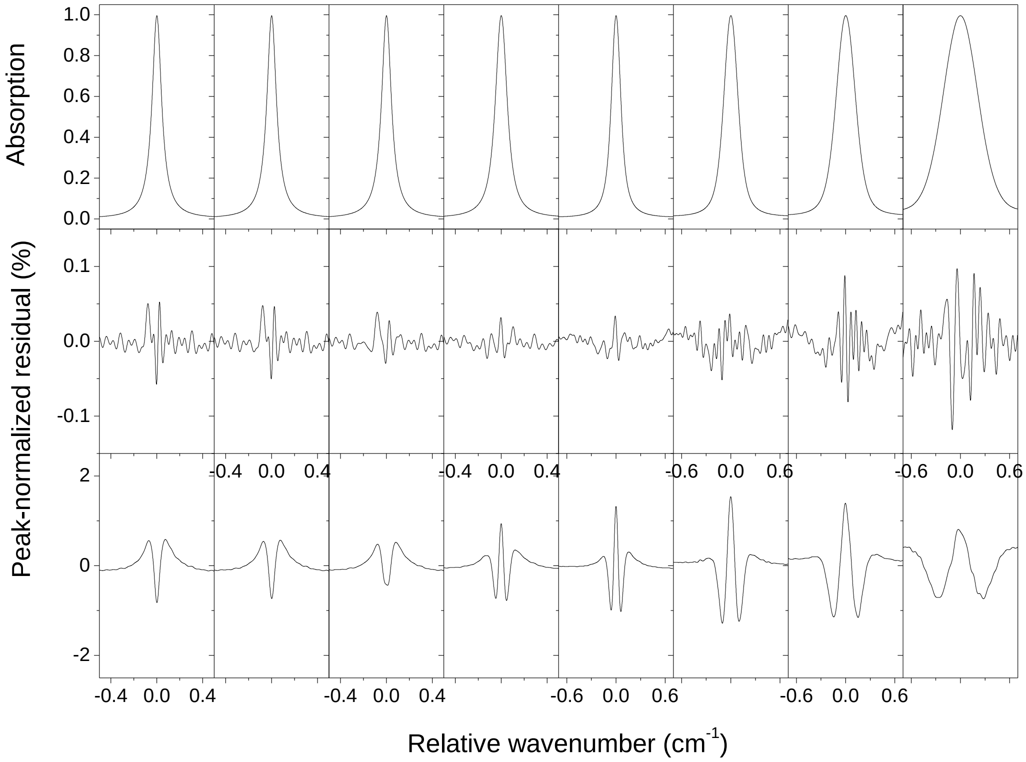

Fig. 3: Example of rCMDS-calculated spectra of N_2-broadened CO_2 (top panel) and the corresponding residual obtained from multi-fits of these spectra with the sdNG profile (middle panel) and with the usual Voigt profile (lowest panel). The example given here is for the P(10) line, calculated at T=200 K, P_{N2}=0.5 atm. From the left to the right, the Doppler width is 0.0023, 0.0046, 0.0091, 0.0274, 0.0382, 0.0764, 0.1145 and 0.2291 cm^{-1}.

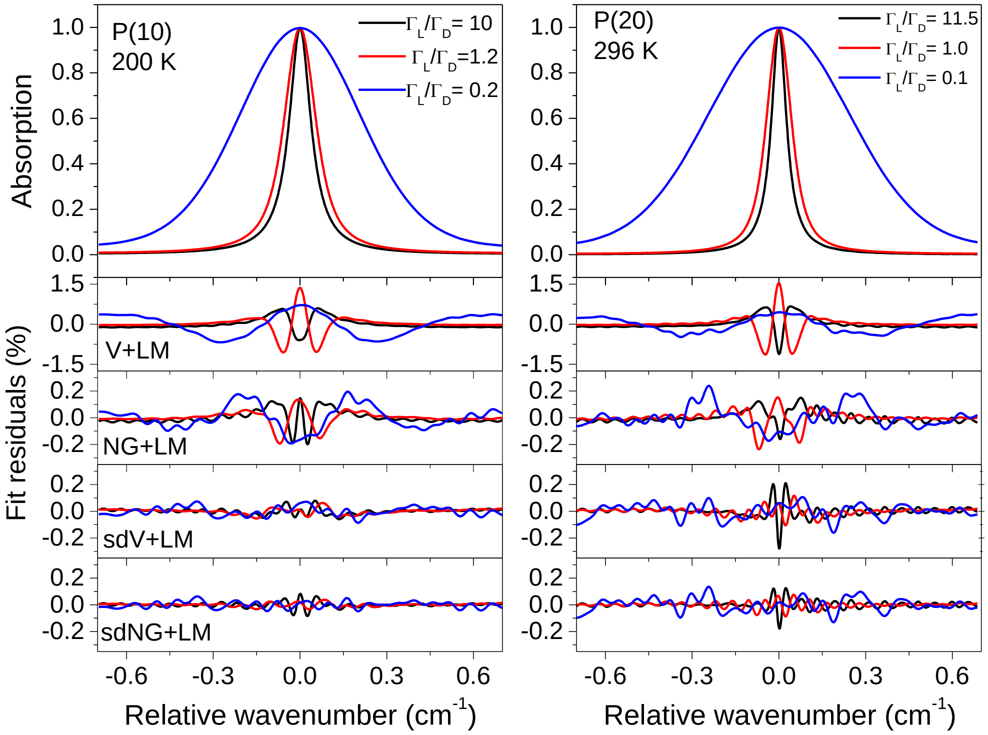

Fig. 4: rCMDS-calculated spectra for the P(10) and P(20) lines of CO_2 broadened by O_2 at 200 K and 296 K, respectively and for different Γ_L/Γ_D ratios, the O_2 pressure being 0.5 atm. In the lower panels are the fit residuals obtained from multi-fitting these spectra with the Voigt (V), the Nelkin-Ghatak (NG), the speed-dependent Voigt (sdV) and the speed-dependent Nelkin-Ghatak (sdNG) profiles. Line-mixing effect was taken into account using the first-order approximation.

Tests were also made with the Hartmann-Tran profile [47,35] in which the correlation between velocity changes and internal state changes is also taken into account. However, the results show no improvement with respect to the sdNG profile. The sdNG model is thus retained for the analysis of the simulated spectra.

3.2 The line-shape paramters and their temperature dependences

Line-shape parameters for N_2/O_2/air-broadened CO_2 lines, deduced from rCMDS-calculated spectra. γ_0, γ_2, β are in cm^{-1}/atm and ζ in atm^{-1}. *Unc* is the total uncertainty (1σ), in units of the last quoted digit.

Line	γ_0	*unc*	γ_2	*unc*	β	*Unc*	ζ	*unc*	n_{γ_0}	*unc*	n_{γ_2}	*unc*	n_{β}	*unc*	n_{ζ}	*unc*
P2	0.0778	3.8	0.0063	3.2	0.0018	3.3	-0.0124	14.5	0.732	1.6	0.441	196	1.940	730	0.436	57
P4	0.0742	3.7	0.0073	3.7	-0.0011	2.4	-0.0105	12.6	0.726	4.6	0.333	312	3.508	1571	0.603	49
P6	0.0720	3.6	0.0068	3.4	0.0000	1.7	-0.0077	14.1	0.722	3.6	0.667	292	0.983	1413	0.675	80
P8	0.0704	3.5	0.0068	3.4	0.0004	1.5	-0.0056	14.5	0.725	2.8	0.767	231	-1.651	2305	0.562	41
P10	0.0690	3.5	0.0062	3.1	0.0010	1.7	-0.0038	12.5	0.724	3.5	0.757	230	0.011	1156	0.558	71
P12	0.0678	3.4	0.0063	3.1	0.0008	1.3	-0.0024	14.0	0.720	3.0	0.497	104	1.282	804	-0.375	124
P14	0.0666	3.3	0.0057	2.8	0.0021	2.3	-0.0005	17.0	0.730	2.6	0.901	235	-0.817	943	-6.247	2281
P16	0.0657	3.3	0.0056	2.8	0.0020	2.4	0.0005	14.5	0.726	2.3	0.522	71	0.899	314	3.503	306
P18	0.0647	3.2	0.0051	2.5	0.0029	3.0	0.0016	12.5	0.730	3.7	0.716	106	0.184	308	2.865	192
P20	0.0640	3.2	0.0049	2.5	0.0028	2.9	0.0028	13.8	0.734	3.4	0.662	39	0.103	293	2.151	143
P22	0.0633	3.2	0.0048	2.4	0.0028	2.9	0.0036	5.6	0.739	1.7	0.685	166	0.009	660	1.894	125
P24	0.0626	3.1	0.0046	2.3	0.0030	3.1	0.0045	6.5	0.741	5.3	0.477	87	0.779	283	1.609	153
P26	0.0621	3.1	0.0049	2.5	0.0018	2.1	0.0062	8.2	0.749	5.1	0.619	231	0.735	623	1.752	168
P28	0.0615	3.1	0.0041	2.1	0.0035	3.6	0.0066	8.6	0.756	4.5	0.640	83	0.172	251	1.440	40
P30	0.0611	3.1	0.0043	2.2	0.0026	2.9	0.0070	9.1	0.757	4.8	0.551	158	0.866	362	1.478	124
P32	0.0606	3.0	0.0040	2.0	0.0036	3.8	0.0078	9.8	0.760	3.6	0.690	113	0.401	399	1.173	65
P34	0.0602	3.0	0.0037	1.9	0.0036	3.8	0.0078	9.8	0.766	7.4	0.843	75	-0.489	358	1.505	80
P36	0.0597	2.9	0.0037	1.9	0.0033	3.6	0.0083	10.4	0.771	5.7	1.156	131	-0.971	447	1.038	136
P38	0.0594	2.9	0.0044	2.2	0.0015	2.4	0.0092	11.3	0.763	4.2	0.253	266	0.976	1339	1.322	113
P40	0.0589	2.9	0.0030	1.6	0.0049	5.2	0.0092	18.1	0.777	4.0	0.883	137	0.020	295	0.942	88
P42	0.0585	2.9	0.0034	1.7	0.0037	4.1	0.0103	12.4	0.773	3.1	0.927	156	-0.751	797	1.146	110
P44	0.0582	2.9	0.0031	1.7	0.0046	5.0	0.0094	11.5	0.768	4.1	0.405	568	1.476	1608	1.003	175
P46	0.0577	2.9	0.0034	1.7	0.0034	4.1	0.0113	13.5	0.768	4.0	-0.083	1131			0.999	186
P48	0.0573	2.9	0.0032	1.7	0.0040	4.8	0.0094	11.6	0.778	5.9	0.335	368	0.158	993	1.293	267
P50	0.0570	2.9	0.0031	1.7	0.0053	6.2	0.0109	13.1	0.786	18.4	0.863	942	0.224	3603	1.249	175

Table 2: Line-shape parameters for O_2-broadened CO_2 lines, deduced from rCMDS-calculated spectra. γ_0,γ_2,β are in cm^{-1}/atm and ζ in atm^{-1}.*Unc* is for the total uncertainty (1σ), in units of the last quoted digit.

Line	γ_0	*unc*	γ_2	*unc*	β	*unc*	ζ	*unc*	n_{γ_0}	*unc*	n_{γ_2}	*unc*	n_β	*unc*	n_ζ	*unc*
P2	0.0883	4.4	0.0071	3.5	0.0007	0.7	-0.0144	21.7	0.738	0.5	0.484	49.5	3.989	366	0.824	111
P4	0.0838	4.2	0.0068	3.4	0.0012	1.2	-0.0132	19.8	0.732	4.3	0.515	1.0	2.367	30	0.662	219
P6	0.0815	4.1	0.0071	3.5	0.0006	0.6	-0.0103	15.5	0.726	2.0	0.374	98.3	2.683	656	0.664	62
P8	0.0798	4.0	0.0069	3.5	0.0014	1.3	-0.0076	11.4	0.718	1.1	0.406	0.5	1.996	594	0.513	243
P10	0.0783	3.9	0.0071	3.5	0.0011	1.0	-0.0048	14.0	0.719	4.9	0.472	96.8	1.501	515	0.676	342
P12	0.0769	3.8	0.0067	3.3	0.0017	1.7	-0.0026	16.0	0.720	2.5	0.532	51.6	1.151	308	-0.031	1408
P14	0.0757	3.8	0.0064	3.2	0.0024	2.4	-0.0014	15.0	0.724	3.0	0.694	123.3	0.259	716	-1.725	680
P16	0.0748	3.7	0.0065	3.2	0.0017	1.7	-0.0000	12.0	0.719	1.9	0.403	24.9	1.851	285	6.236	549
P18	0.0739	3.7	0.0060	3.0	0.0029	2.8	0.0016	9.0	0.722	2.2	0.532	88.5	0.984	519	2.304	423
P20	0.0731	3.7	0.0059	3.0	0.0028	2.8	0.0023	8.0	0.721	4.4	0.476	54.5	0.992	48	2.729	157
P22	0.0724	3.6	0.0061	3.1	0.0022	2.2	0.0041	6.2	0.723	3.7	0.458	17.9	0.997	192	1.870	182
P24	0.0717	3.6	0.0055	2.8	0.0035	3.5	0.0050	7.5	0.728	2.0	0.542	94.1	0.406	294	2.033	107
P26	0.0711	3.6	0.0056	2.8	0.0028	2.7	0.0064	9.7	0.733	5.4	0.664	25.3	-0.070	228	1.629	67
P28	0.0704	3.5	0.0050	2.5	0.0039	3.9	0.0070	10.5	0.738	5.3	0.627	16.5	0.365	92	1.566	40
P30	0.0700	3.5	0.0054	2.7	0.0030	2.9	0.0077	11.6	0.737	6.0	0.595	21.6	0.383	189	1.544	76
P32	0.0695	3.5	0.0052	2.6	0.0033	3.2	0.0088	13.2	0.732	1.9	0.412	186.2	1.026	874	1.376	44
P34	0.0690	3.5	0.0053	2.7	0.0025	2.4	0.0092	13.8	0.745	6.6	0.510	65.9	0.650	349	1.540	111
P36	0.0684	3.4	0.0048	2.4	0.0035	3.4	0.0088	13.2	0.744	1.0	0.549	118.9	0.535	432	1.549	32
P38	0.0680	3.4	0.0051	2.5	0.0023	2.2	0.0093	14.0	0.740	2.2	0.334	85.5	1.352	411	1.404	349
P40	0.0676	3.4	0.0048	2.4	0.0033	3.2	0.0102	15.4	0.744	0.5	0.514	78.9	0.372	656	1.218	205
P42	0.0670	3.4	0.0042	2.1	0.0047	4.7	0.0113	16.9	0.756	5.9	0.954	72.6	-1.170	526	1.313	394
P44	0.0667	3.3	0.0046	2.3	0.0033	3.2	0.0108	16.3	0.730	4.4	0.214	147.1	1.798	282	0.955	368
P46	0.0661	3.3	0.0043	2.1	0.0033	3.3	0.0105	15.8	0.734	5.8	-0.319	347.0	3.393	473	1.882	131
P48	0.0659	3.3	0.0047	2.3	0.0023	2.2	0.0111	16.7	0.743	11.7	0.409	9.8	1.389	39	1.306	424
P50	0.0655	3.3	0.0044	2.2	0.0036	3.5	0.0108	16.4	0.726	5.9	0.924	180.8	0.231	998	2.822	475

Table 3: The same as Table 2 but for air-broadened CO_2.

All the calculated line-shape parameters including $\gamma_0, \gamma_2, \beta$ or ζ and their temperature dependence exponent n also were compared with other experiment data as shown in some Figures below.

- **Line broadening coefficients and their temperature dependences**

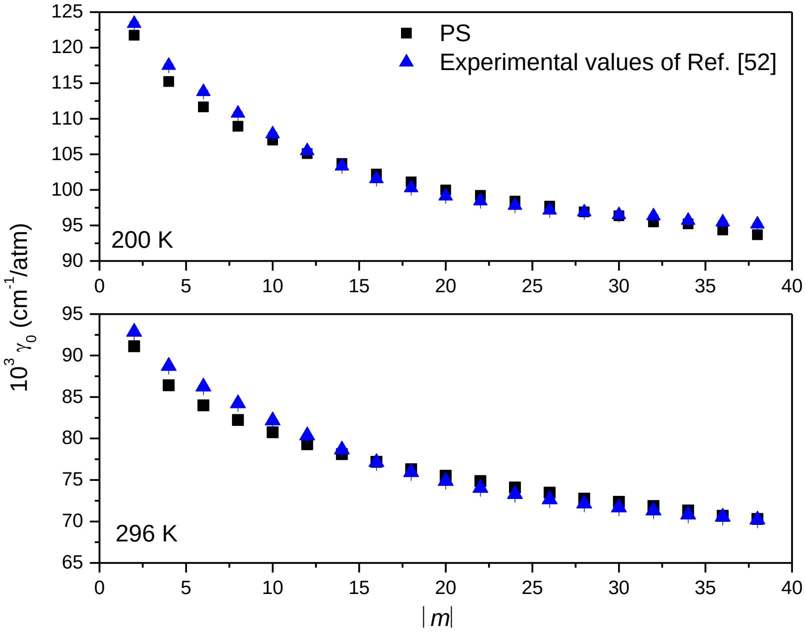

Fig. 5: Comparison between line broadening coefficients deduced from fit of rCMDS-calculated spectra (present study-PS, black squares) with the HT profile and those of [52] (blue triangles), obtained from fits of FTS measurements with the same profile. In the lower and upper layers are results at 296 K and 200 K, respectively.

Figure 5 shows comparisons between the N_2-broadening coefficient, γ_0, of CO_2 lines obtained from our calculations and those retrieved from experimental spectra [52] versus the rotational quantum number $|m|$ ($m = -J$ and $m = J + 1$ for P and R branches lines, respectively, with J the rotational quantum number of the lower level of the line), for 200 K and 296 K. For lines with $|m|$ greater than 40, due to their weak signal-to-noise ratio, it was impossible to fit the rCMDS-calculated spectra with the sdNG profile. As mentioned in the previous section, the values at a given temperature were obtained directly from fits of rCMDS-spectra calculated at the same temperature. The uncertainties of the rCMDS-predicted values are not reported here since it is almost impossible to accurately determine them. Indeed, this would require the determination of those due to the used intermolecular potential, to the numerical approaches used in the rCMDS, to the retrieval of the parameters searched for in the fits. For the experimental data, the values of $\gamma_0(296\,K)$ and the corresponding uncertainties were directly taken from the supplementary data of [52] while $\gamma_0(200\,K)$ were calculated using the power law [Eq. (3)] with the temperature exponents, n_{γ_0}, also given in the supplementary data of [52]. As can be seen in Fig. 3a, our CMDS-deduced γ_0 are in very good agreement with the experimental ones, for both temperature conditions. The averaged differences are 0.9 (±0.6) % and 1.1 (±0.8) % at 200 K and 296 K, respectively.

The retrieved broadening coefficients for O_2-broadened CO_2 lines are presented in the right part of Fig. 6 versus the rotational quantum number $|m|$ ($m = -J$ for P branch lines, J being the rotational quantum number of the lower level of the line) for the four considered temperatures. Due to their weak signal-to-noise ratio, broadening coefficient for lines with $|m|$ greater than 60 could not be determined. Several studies in the literature were devoted to the measurements of the O_2-broadening coefficients of CO_2 lines (see [77] and references therein). Most of them employed the Voigt profile to model the measured spectra, except [77] and [78]. In [77], the speed-dependent Voigt profile was used to retrieve the O_2-broadened CO_2 line-shape parameters in the 30013←00001 and 30012←00001 bands from high-resolution FTS spectra of CO_2 lines. Hikida and Yamada [78] used the Galatry profile to determine O_2-broadening coefficients for ten CO_2 lines in the 30013←00001 band from diode laser measurements. It is well known that using the Voigt profile leads to smaller retrieved line broadening coefficients with respect to more refined line-shape models. Therefore, only [77] and [78] are retained here for comparison with our predicted results (left part of Fig. 6), both the measured and calculated values were obtained at room temperature. As can be observed, our predicted values are in rather good agreement with measured results, with an average difference of about 2%, a very satisfying result for a classical method.

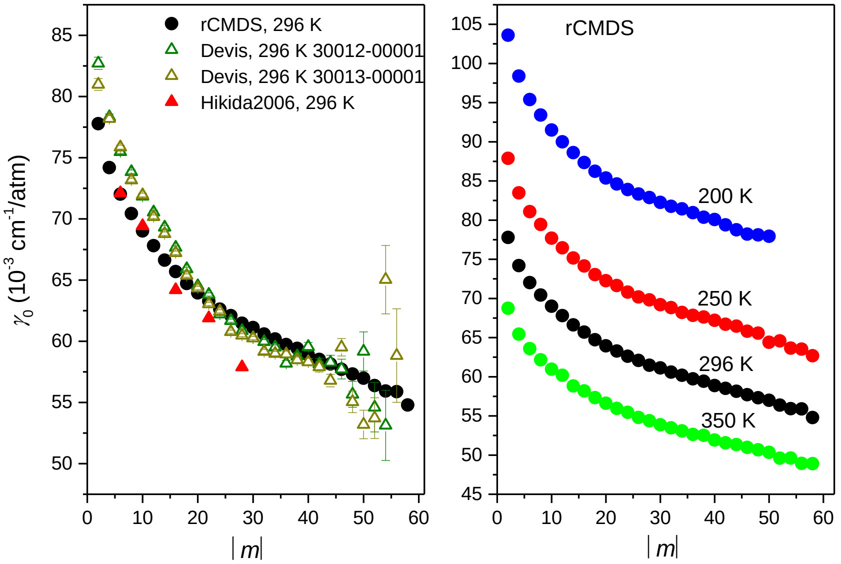

Fig. 6: Left panel: O_2-broadening coefficients of CO_2 lines deduced from fits of rCMDS-calculated spectra at 296 K (black circles) with the sdNG profile and comparison with measured values of [77] (olive and dark yellow triangles for the 30012←00001 and 30013←00001 bands, respectively) and [78] (red triangles)

Right panel: rCMDS-predicted broadening coefficients of CO_2 in O_2 at 200, 250, 296 and 350 K.

The predicted broadening coefficients for CO_2/O_2 at 200, 250 and 296 K are then combined with those of CO_2/N_2 at the same temperature conditions to deduce the air-broadening coefficients using $\gamma_0^{air}(T) = 0.79\gamma_0^{N2}(T) + 0.21\gamma_0^{O2}(T)$. Figure 7 shows the obtained air-broadening coefficients for the three considered temperatures and their comparison with data of [65], [68] and of [66,56]. In those studies, air-broadening coefficients were determined from fits of measured spectra using the sdNG [68], the partially-correlated speed-dependent Nelkin-Ghatak (pcsdNG) [65] and the sdV [66,56] profiles. We can reasonably compare values of γ_0 obtained with these various speed-dependent profiles since, as demonstrated in [95], the differences between values of γ_0 obtained with these speed-dependent profiles are very small, below 1%. In [68] only the R(16) line of the 30013←00001 band was measured but for various temperatures. Values of γ_0 for 36 lines in the 30012←00001 band were measured in [65] at room temperature. In [66], lines of various vibrational bands in the 2.06 μm spectral region were measured at various temperatures, only parameters of the most intense band (20013←00001) being shown here. Finally, [56] was devoted to the (30013←00001) band of CO_2. Values of [68] and [66,56] at 250 and 200 K were deduced from the coefficients given at room temperature and the temperature dependence exponents. As shown in Fig. 7, a very good agreement between our predictions and these data can be observed. Most of the measured data are in good agreement with the predictions, except for values at low $|m|$ where the difference between our prediction and measured values of [66] can be up to 5%. These results confirms the quality of predictions using requantized CMDS and the associated intermolecular potential.

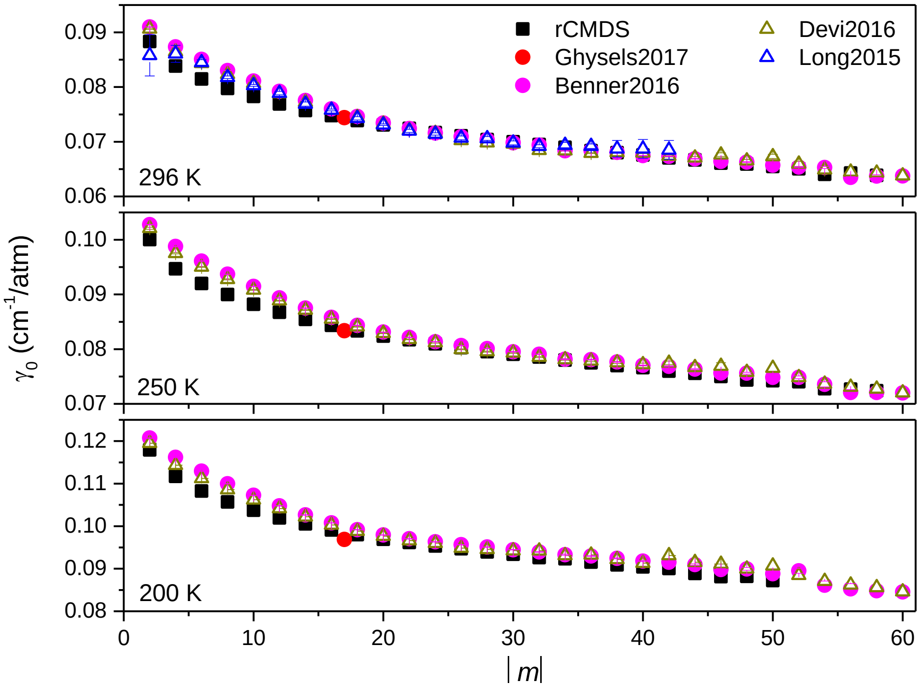

Fig.7: Air-broadening coefficients predicted by rCMDS at 296, 250 and 200 K. Results of [68], [65], and [66,56], obtained from fits of measured spectra with respectively, the sdNG, pcsdNG and sdV profiles, are also displayed for comparison.

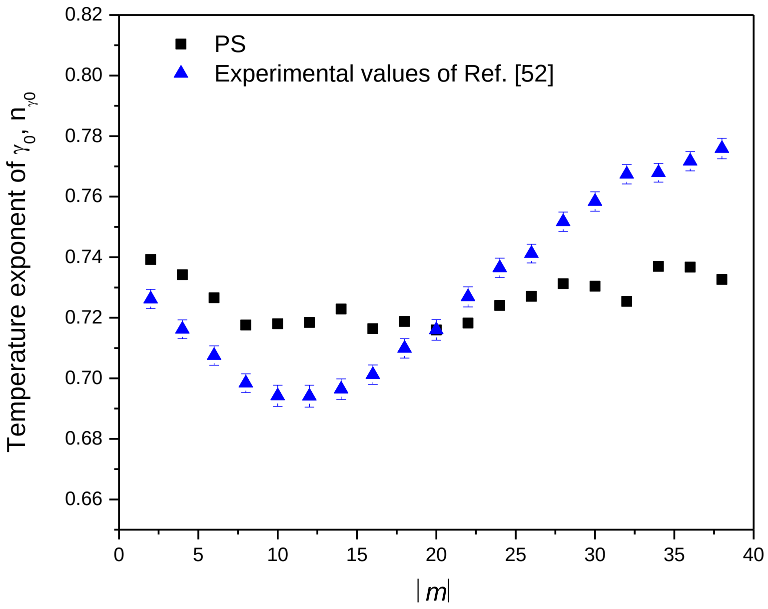

Fig. 8: The temperature exponent parameter for the broadening coefficient of N_2-broadened CO_2 lines, predicted from rCMDS and comparison with measured values of [52]

Figure 8 shows the comparison between the temperature exponent n_{γ_0} deduced from rCMDs calculations and the experimental values [52]. As can be observed, for $|m| > 20$, the predicted values of n_{γ_0} is smaller than the experimental value while it is larger for $|m| < 20$. The "non-smooth" behavior of rCMDS-deduced n_{γ_0} with $|m|$ is probably due to the limited signal-to-noise ratio of the calculated spectra but also to the limited values of temperature considered in the calculations (i.e. at 200 and 296 K only). They also give an idea about the uncertainty of your predicted values. Overall, the average difference between the rCMDS-deduced values and those of [52] is 2.9 (±1.5) %. Starting from the same values of the line-broadening coefficient γ_0 at reference temperature (i.e. 296 K), this difference in n_{γ_0} corresponds to a mean difference of about 1 % on the values of γ_0 at 200 K, for instance.

The temperature dependences for O_2- and air-broadening coefficients are determined using the usual power law. The obtained results are displayed in Fig. 9, together with data for CO_2/air of [68] and [66,56] but also those given in the 2016 edition of the HITRAN database [79]. For completeness, experimental values of [69] for N_2-broadened CO_2 lines in the ν_3 band, obtained with the use of the sdNG profile, are also reported. For the predicted values, error bars obtained from the standard uncertainty of the fits (1σ) for the temperature exponents are also displayed. As can be seen on Fig. 9, our predicted values for O_2 and air-broadening are quite close to each other, the maximum difference being for high $|m|$. For air-broadening, all the plotted data including the predicted ones are in good agreement, within 7-8%. This demonstrates that rCMDS can be fully used to predict the temperature dependences of the broadening coefficients for molecular systems such as CO_2. The rCMDS predicted values of $\gamma_0(296\,K)$ and n_{γ_0} are listed in Table 2 and 3 for O_2- and air-broadening, respectively.

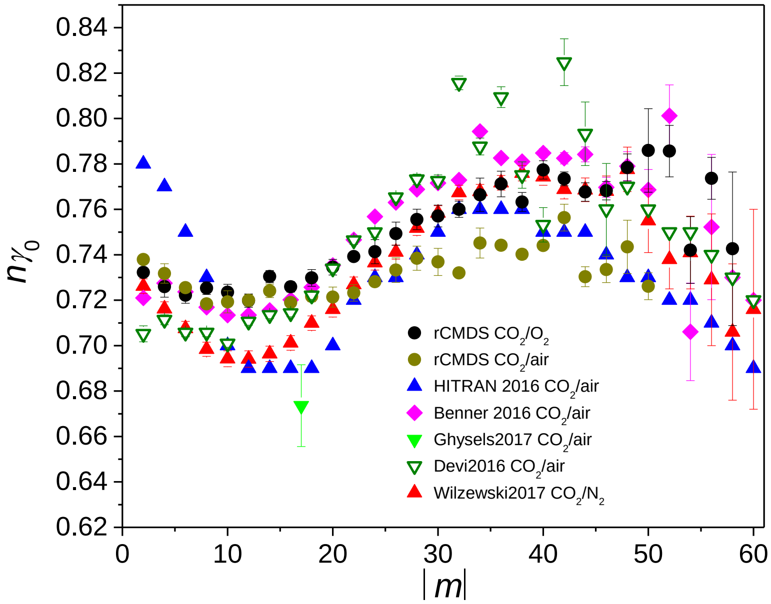

Fig. 9: The temperature exponents of O_2- (black circles) and air-broadening (olive circles) coefficients of CO_2, deduced from rCMDS vs |m| and comparison with those for CO_2 in air of [66] (purple diamonds), [68] (green triangles), [56] (olive triangles) and [79] (blue triangles) and for CO_2 in N_2 of [69] (red triangles).

- **The speed dependence of the line width and its temperature dependence**

The rCMDS-predicted values for the speed dependence parameters γ_2 are plotted in Fig. 10a for the two considered temperatures. Experimental values of [52] are also reported. As can be observed, a very good agreement between the predicted and experimental values of γ_2 is obtained. Their average difference is only 5 and 10 % at 296 K and 200 K, respectively. This is the first time that this high-order line-shape parameter is predicted from purely theoretical calculations with this precision. From the values of γ_2 obtained at 200 K and 296 K, we then computed the temperature exponent n_{γ_2} [see Eq .(3)] which are plotted in Fig. 10b, together with those deduced from measured spectra [52]. As can be seen, the theoretical and experimental results are in rather good agreement, with mean values (averaged over all the considered rotational quantum numbers) of 0.51 and 0.46, respectively. Again, recall that the part of the line-to-line variations of the predicted parameters is not physically meaningful and results from the noise on the calculated spectra, as obvious for n_{γ_2}.

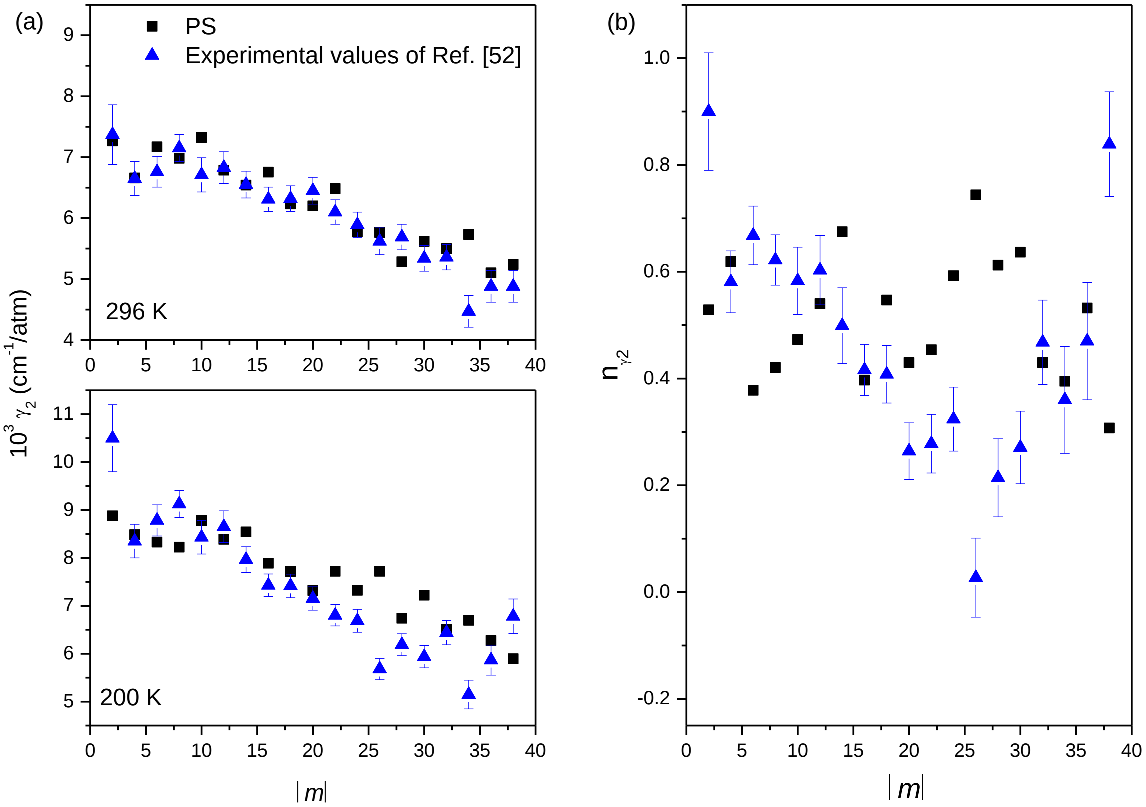

Fig. 10: Comparison between the speed dependence parameter γ_2 (left panel) and the temperature dependence (right panel), predicted from rCMDS and the experimental values of [52] of CO_2-N2

As for γ_0, the temperature dependences for γ_2 are also modeled by the power law. From values of γ_2 predicted by rCMDS at various temperatures, n_{γ_2} for O_2- and air-broadening are thus deduced and plotted in Fig. 11, together with their statistical uncertainty obtained from the fits. For comparison, the rCMDS-predicted values for n_{γ_0} (see Fig. 9) are also displayed. For O_2-broadening, the values of n_{γ_2} are determined with large uncertainty and randomly vary between the 0.05-1.2 range. For air-broadening, the variation with $|m|$ of n_{γ_2} is much less random. It is clearly shown that for CO_2 in air, the temperature dependence of γ_2 is weaker than that of γ_0, which is consistent with the observation of [69] for CO_2 in N_2. This difference with Eq. (3) shows the limit of the phenomenological quadratic speed dependence and probably also of the power law for the temperature dependence. These models should thus be considered as effective with different temperature dependences for γ_0 and γ_2.

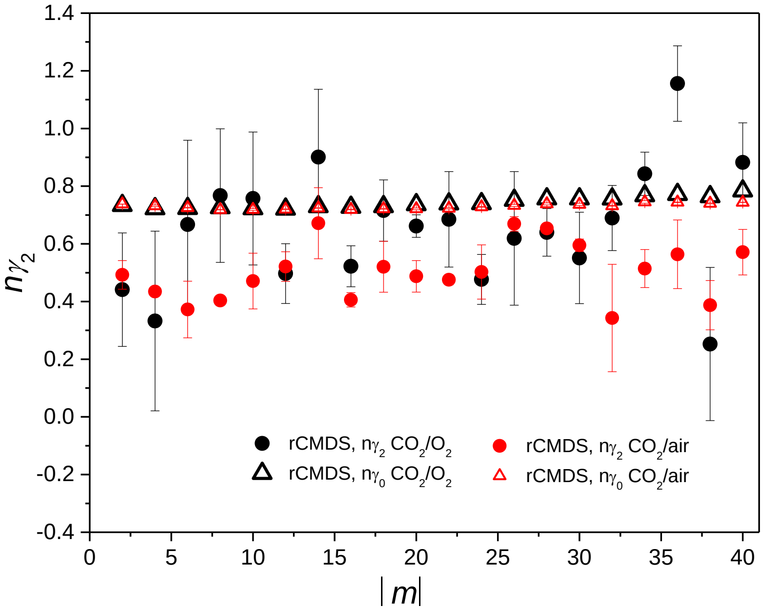

Fig. 11. The temperature exponents of the speed dependence parameters, n_{γ_2}, for O_2- (red circles) and air-broadened (black circles) CO_2. n_{γ_0} are also displayed for comparison. The plotted error bars correspond to the uncertainty (1σ) obtained from the fits of the temperature exponents.

- **The Dicke narrowing parameter and its temperature dependence**

The rCMDS-predicted Dicke narrowing parameters obtained at 200 K and 296 K are presented in Fig. 9a, together with the experimental values of [52] while the corresponding temperature exponents are plotted in Fig. 9b. As can be observed in Fig. 12a, the same rotational dependence (i.e. β increases with increasing rotational quantum number) is observed for the experimental and rCMDS-predicted values of β. However, our calculated values are much smaller than those of [52]. In the considered pressure range, the impact of this parameter on the measured spectra is much smaller than that of other parameters such as γ_0, γ_2 or ζ. This explains that the relative experimental uncertainty of this parameter is much larger than that of the other parameters (see also Fig. 12 of [52]). We can assume that the uncertainty on the rCMDS-predicted parameters is more or less on the same order as for the experimental values [52] due to similar signal-to-noise ratios of the measured and calculated spectra. Within these uncertainties, the measured and rCMDS-predicted values of β (as well as the temperature dependence exponents) are rather in good agreement.

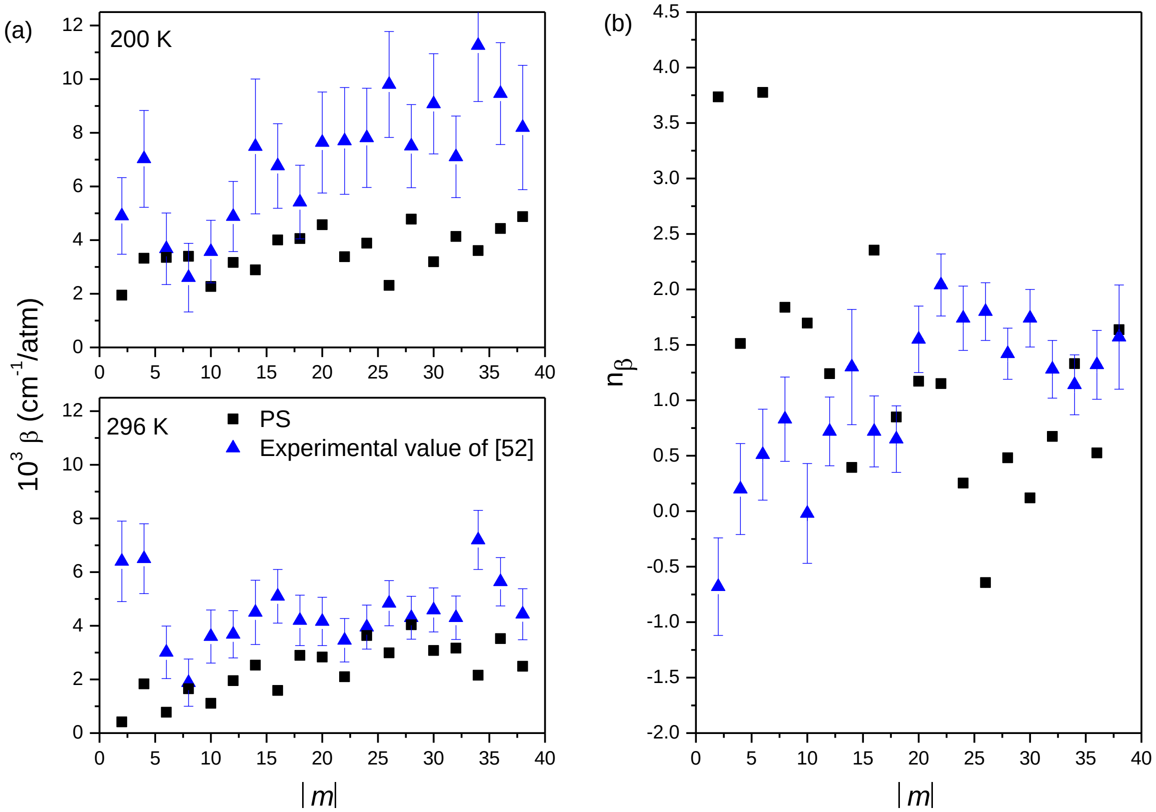

Fig. 12: The same as figure 10 but for the Dicke narrowing coefficient β.

The retrieved Dicke narrowing parameters, β, for all the considered temperatures are presented in the left panel of Fig. 13 for both CO_2/O_2 and CO_2/air. Recall that results for CO_2 in air were determined from results for CO_2/O_2 and for CO_2/N_2. It is well known that the Dicke narrowing coefficient strongly depends on the line-shape model used to fit the measured/simulated spectra. For the same line, values obtained with the Nelkin-Ghatak, the speed-dependent Nelkin-Ghatak and the partially-correlated speed-dependent Nelkin-Ghatak profiles could be completely different. To the best of our knowledge, there is no available data for β, obtained with the sdNG profile for O_2- and air-broadened CO_2, except [68] in which no value of β can be found. The rCMDS-predicted values of β (left panel of Fig. 13) are rather small compared to those of γ_0 and γ_2. In fact, as can be observed in Fig. 4, including the Dicke narrowing effect improves only slightly the fit residuals. The determined values are small and largely influenced by the signal to noise ratio of the calculated spectra. The 1σ combined uncertainty for β is about 10-20%. As a consequence, the deduced temperature dependence of the Dicke narrowing parameter, n_β, is associated with large error bars (right panel of Fig. 13). The values of n_β from [69], determined from fits of measured spectra with the sdNG profile, but for CO_2/N_2 are also reported here for comparison.

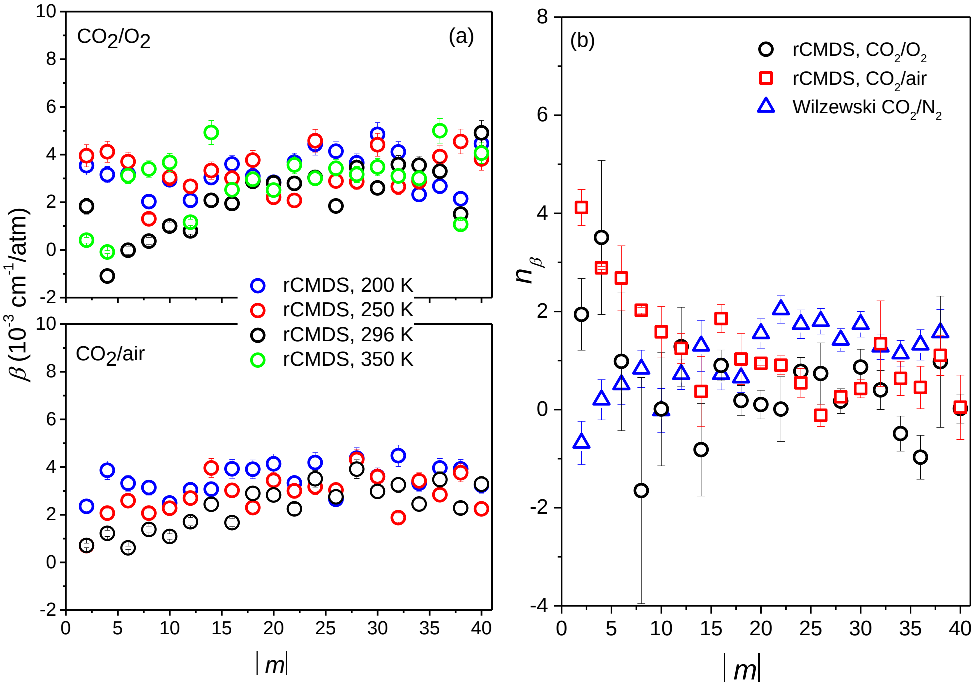

***Fig. 13**:* Left panel: the rCMDS-predicted Dicke narrowing parameters for O_2 and air-broadened CO_2 for all the considered temperatures.
Right panel: the deduced temperature exponents of the Dicke narrowing parameters for O_2- and air-broadened CO_2 lines and comparison with measurement-deduced values of [69] for CO_2/N_2.

- **The first-order line-mixing parameter and its temperature dependence**

The comparison between the rCMDS-predicted first-order line-mixing parameters and the experimental values [52] for T = 200 and 296 K is shown in Fig. 14a while the corresponding temperature dependence exponents are compared in Fig. 12b. As shown in Fig. 14a, a very good agreement between the rCMDS-predicted and experimental values of ζ is observed for the two temperatures. Note that, in the requantization procedure used in our CMDS, we did not take into account the centrifugal distortion effect. Therefore, in the resulting rCMDS spectra, the successive P(J) lines are equally spaced which is not the case in the true ν_3 band of CO_2. This problem can be corrected by imposing directly the true rotational line positions, taken from a spectroscopic database [79], as done in [93]. However, Fig. 14a shows that, although the relative line positions of rCMDS calculated spectra are slightly different of the true ones, the first-order line-mixing parameters [75] (which depend on the relative line positions) predicted are in very good agreement with measured values. Fig. 14b shows that the temperature dependence exponents predicted are also in good agreement with the experimental values [52]

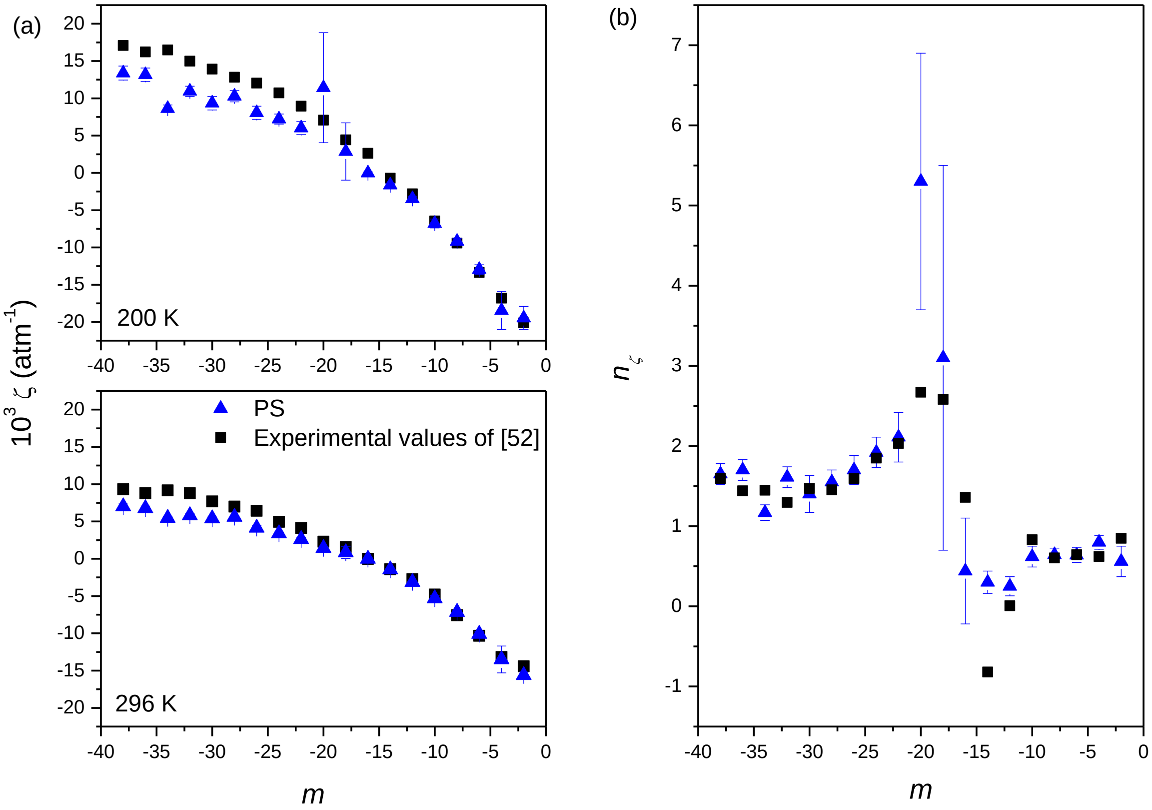

Fig. 14: The same as figure 10 but for the first-order line-mixing parameter ζ.

Line-mixing effect in CO_2 spectra is of great importance for applications such as atmospheric remote sensing studies (see [37,80] for instance). Various studies were devoted to the calculations and/or measurements of either the first-order line-mixing coefficients or the off-diagonal elements of the relaxation matrix for CO_2 (e.g. [65,66,67,56,80]. The rCMDS predicted first-order line-mixing parameters, ζ, for O_2-broadened CO_2 for the four considered temperatures are plotted in the left part of Fig. 15. For air-broadened CO_2, the values of ζ were determined as a combination of those for O_2- and N_2-broadening are shown in the right part of Fig. 15. Our predicted values are compared with measured values of [81] for the 30012←00001 and 30013←00001 bands, obtained with the sdV profile and with those of [65] for the 30012←00001 band, with the pcsdNG profile. The first-order line-mixing parameters deduced from the modeled relaxation matrix of [80] at 296 and 200 K for the ν_3 band are also displayed for comparison. For $|m| \leq 30$ a very good agreement with the measured values is observed while for higher values of $|m|$, the rCMDS-predicted values are larger than the measured and calculated values. Note that the difference with measured values cannot be explained by the difference in the used line profiles since it was observed that the first-order line-mixing parameter does not significantly depend on the line shape (see [94,81] for instance). A possible source of difference could be our requantization scheme. In fact, in the requantization procedure used in our CMDS, we did not take into account the centrifugal distortion effect. As a result, the successive $P(J)$ line are equally spaced in the rCMDS-calculated spectra, which is not the case for a vibrational band of CO_2.

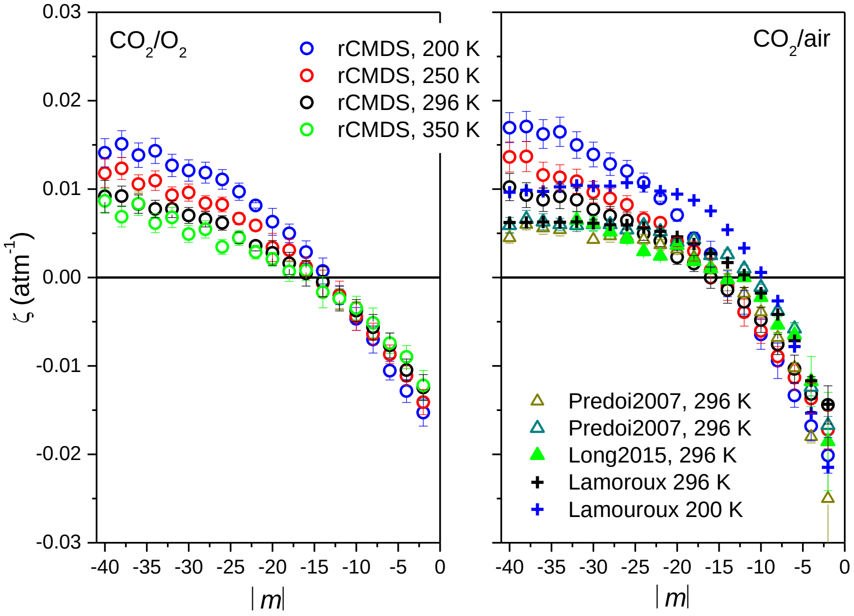

Fig.15: Left panel: first-order line-mixing parameters predicted from rCMDS for O_2-broadened CO_2 at 200, 250, 296 and 350 K.

Right panel: air-broadened first-order line-mixing parameters for CO_2, calculated from the present rCMDS-predicted values for CO_2/O_2 and those of CO_2/N_2 [70] at 200, 250 and 296 K. Measured values for CO_2 in air of [81] for the 30012←00001 (dark cyan) and 30013←00001 (dark yellow) bands, obtained with the sdV profile and those of [65] for the (30012←00001) band, with the pcsdNG profile are reported for comparison. Values deduced from the modeled relaxation matrix of [80] for the ν_3 band at 296 and 200 K are also displayed.

The temperature dependence of the rCMDS-predicted ζ is presented in Fig. 16 for both CO_2/O_2 and CO_2/air. The plotted error bar is the uncertainty due to the fit of the temperature exponents which take the uncertainty of $\zeta(T)$ into account. As can be observed, there is no significant difference between n_ζ for O_2- and air-broadening and they are in good agreement with the experimental values of [69] for CO_2 in N_2

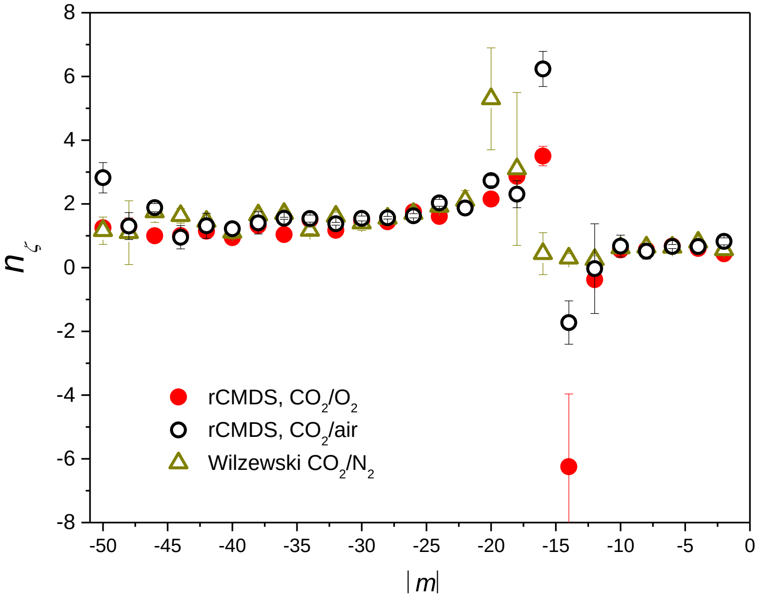

Fig.16: The temperature dependences of the first-order line-mixing parameters predicted by rCMDS for CO_2/O_2 and CO_2/air. Values of [69] for CO_2/N_2 are also displayed for comparison

For the calculations with N_2O in air:

The same method was used to deduce all the predicted line-shape parameters and their temperature dependence. Classical molecular dynamics simulations (CMDS) were performed at 1 atm and three temperatures 200, 250 and 296 K for N_2O-air mixtures with 50% of air, which contains 80% of N_2 and 20% of O_2 molecules. In which, for the rCMDS, only interactions between N_2O and N_2, N_2O and O_2 were authorized in the calculations. This is equivalent of simulating a system in which N_2O molecules are highly diluted in 0.5 atm of air. The molecules are considered as rigid rotors. A site-site functional form with Coulombic and atom-atom contributions was used to represent the interaction potentials between N_2O and N_2, and N_2O and O_2 molecules. The molecular geometries and the charges and sites were taken from [92] for N_2O and from [73] for N_2 and O_2 molecules. The atom-atom contribution was calculated as a 12-6 Lennard-Jones potential whose parameters were calculated using the Lorentz-Berthelot combination rules and parameters of N_2O-N_2O [92] and N_2-N_2 and O_2-O_2 [73] interactions. The obtained spectra were then fitted with the quadratic speed-dependent Voigt profile including the first-order line mixing using a multi-spectrum fitting procedure. Comparisons with values determined from room temperature high-precision measurements in the ν_3 band of N_2O with the same profile [97] showed that our retrieved line broadening coefficients are overestimated by about 5%. The ratio between the measured and predicted line broadening coefficients were thus used to empirically correct the rCMDS-calculated auto-correlation functions and thus the corresponding absorption spectra. These latter were then fitted with the Voigt, speed-dependent Voigt and speed-dependent Nelkin-Ghatak profiles, associated with the first-order line-mixing approximation, providing the corresponding line-shape parameters for lines up to $J'' \leq 60$. The temperature dependences of various line-shape parameters were also deduced. The results show a very good agreement with available experimental data for all the considered parameters.

III. Conclusions

In the first two years (from 9/2018 to 12/2020), under the careful guide of the two supervisors, I have studied acquired different skills in the study of infrared molecular spectroscopy: using a rCMDS to simulate spectra of CO_2 and N_2O diluted in O_2, N_2 with various conditions of pressure and temperature and analysing the simulated data with different line-shape models.

As a result, spectra of the up to 50 transitions of each molecule have been simulated. Line-shape parameters were deduced by fitting the simulated spectra with the quadratic speed-dependent Nelkin– Ghatak profile and also by using other different line-shape models: Voigt, quadratic speed dependent Voigt and Hartmann-Tran (HT) profiles. The collisional broadening coefficient, its speed dependence, the Dicke narrowing and the first-order line-mixing parameters were retrieved using a multi-spectrum fitting procedure. The temperature dependences of these parameters were obtained using the usual single power law. The obtained parameters for CO_2/O_2 were then combined with those of CO_2/N_2 to deduce parameters for CO_2 in air. These results also were compared with other measurented data. The good agreement residuals confirmed that rCMDS can be used as a powerful tool, complementary to high quality measurements, to address the precision and accuracy requirements of application such as atmospheric remote sensing as well as for populating spectroscopic databases with refined line-shape parameters.

The results with N_2O have been done and are being in the preparation of writing paper.

In the next part of this PhD project, the student will continue to improve rCMDS to simulate spectra of other molecules including CH_3Cl and H_2O perturbed by various collision partners at different pressures and at large range of temperature.

IV. Summary of scientific activities and future working plan

1. Scientific working plan (for 3 years, from 2018 to 2021)

Time	Work
5/2018-8/2018	- Study about rCMDS to simulate spectra of linear molecule such as CO_2 deluted in N_2 - Simulate the spectra of CO_2 in N_2 at 296K and other temperatures
8/2018-10/2018	-Learning of a theoretical study about line-shape profiles: Voigt, Rautian, Galatry, speed dependence Voigt profiles, speed dependence N-K and HTr profile
10/2018-12/2019	- Analysis of the measured data of CO_2 diluted in N_2 using these line-shape profiles - Preparing a paper: "**Prediction of line shapes parameters and their temperature dependences for** CO_2- N_2 **using molecular dynamics simulations"**
01/2019-11/2019	- Simulate the spectra of CO_2 in O_2 at 296K and other temperatures - From the results of CO_2 in N_2 and CO_2 in O_2, deduce the results for CO_2 in air - Preparing a paper: **"Line-shape parameters and their temperature dependences predicted from molecular dynamics simulations for O_2- and air-broadened CO_2 lines"**
11/2019-12/2020	- Study about rCMDS to simulate spectra of N_2O deluted in N_2, O_2 and air - Analysis of the measured data of N2O diluted in N_2, O_2 using these line-shape profiles - Preparing a paper: **"Prediction of line-shape parameters and their temperature dependences for air-broadened N_2O linesusing requantized classical molecular dynamics simulations"**
1/2021-08/2021	- Using rCMDS to simulate CH_3Cl and H_2O - Writing the thesis
09/2021-12/2021	- General analysis, conclusions and perspectives - Writing the thesis - Preparing to defend the thesis

2. **Scientific activities** (up to October 2020)

1.	Vietnam School of Earth Observation 2018 – Recontres du Vietnam-USTH-CNES (2018) **Poster:** “Precise predictions of H2O line shapes over a wide pressure range using simulations corrected by a single measurement”
2.	The 10th internaltional conference on photonics and applications (**ICPA-10**) **Poster:** - “New intensity measurements of Carbon Dioxide in the 1.6μm region” - “Model Keilson-Storer and the spectroscopic parameters in the near-infrared of the pure water vapor with Hartmann-Tran profile”
3.	Doctoral Day 2019-USTH **Oral talk**: “Precise modelling of the infrared spectra of carbon dioxide and of water vapor for atmospheric remote sensing”
4.	HRMS 2019, 2019 - Dijon, France **Poster:** - “Precise predictions of H_2O line shaps over a wide pressure range using simulations corrected by a single measurement” - “Prediction of line shaphe parameters and their temperature dependences for CO_2-air using molecular dynamics simulations”
5.	The 11th internaltional conference on photonics and applications (**ICPA-11**) **Poster: “**Prediction of air-broadened N_2O lines using classical molecular dynamics simulations**”**

3. **Publication** (up to October 2020)

1. N.H. Ngo, **H.T. Nguyen**, H. Tran, *Precise predictions of* H_2O *line shapes over a wide pressure range using simulations corrected by a single measurement*, Journal of Quantitative Spectroscopy & Radiative Transfer 207 (2018) 16–22.

2. **H. T. Nguyen**, N. H. Ngo, and H. Tran. *Prediction of line shapes parameters and their temperature dependences for CO2-N2 using molecular dynamics simulations,* J. Chem. Phys. 149, 224301 (2018)

3. **H. T. Nguyen**, N. H. Ngo, and H. Tran. *Line-shape parameters and their temperature dependences predicted from molecular dynamics simulations for* O_2*- and air-broadened* CO_2 *lines*, J. Chem. Phys. 242, 106729 (2020)

02 papers on ICPA-10

1. **Nguyen Thi Huyen Trang**, Le Cong Tuong, Ngo Ngoc Hoa; *Model Kelson-Storer and the spectroscopic paramters in the near-infrared of pure water vapor.* Advances in Optics Photonics Spectroscopy and Applications X; 2019; 125
2. Ngo Ngoc Hoa, P.Chelin, X. Landsheere, M. Schwell, **Nguyen Thi Huyen Trang**, Le Cong Tuong. *New measurements of Carbon Dioxide absorption in the 1.6micrometer region.* Advances in Optics Photonics Spectroscopy and Applications X; 2019; 25

Refrences

[1] A. Rozanov, K. Weigel, H. Bovensmann, S. Dhomse, K.-U. Eichmann, R. Kivi, V. Rozanov, H. Vomel, M. Weber and J. P. Burrows. Retrieval of water vapor vertical distributions in the upper troposphere and the lower stratosphere from SCIAMACHY limb measurements. Atmospheric Measurement techniques **4** 933–954 (2011).

[2] A.D. Bykov, N.N. Lavrentieva, V.N. Saveliev, L.N. Sinitsa, C. Camy-Peyret, Ch. Claveau, and A. Valentin. Half-width temperature dependence of nitrogen broadened lines in the ν_2 band of H_2O. Journal of Molecular Spectroscopy **224** 164–175 (2004).

[3] A.P. Thorne, U. Litzén, and S. Johansson. Spectrophysics : Principles and Applications. Springer, 1999.

[4] C. Claveau, A. Henry, D. Hurtmans, A. Valentin. Narrowing and broadening parameters of H_2O lines perturbed by He, Ne, Ar, Kr and nitrogen in the spectral range 1850-2140 cm^{-1}. Journal of Quantitative Spectroscopy & Radiative Transfer **68** 273-298 (2001).

[5] C.E. Sioris, J. Zou, C.T. McElroy, C.A. McLinden, H. Vömel. High vertical resolution water vapour profiles in the upper troposphere and lower stratosphere retrieved from MAESTRO solar occultation spectra Advances in Space Research 46 (2010) 642–650 (2010).

[6] Chris D. Boone, Kaley A. Walker, Peter F. Bernath, Speed-dependent Voigt profile for water vapor in infrared remote sensing applications. Journal of Quantitative Spectroscopy & Radiative Transfer **105** 525-532 (2007).

[7] D. Lisak, A. Cygan, D. Bermejo, J.L. Domenech, J.T. Hodges, H. Tran. Application of the Hartmann-Tran profile to analysis of H_2O spectra. Journal of Quantitative Spectroscopy & Radiative Transfer, 164, 221- 230 (2015)

[8] D. Lisak, G. Rusciano, A. Sasso. Anaccurate comparison of line-shape models on H_2O lines in the spectral region around 3 μm. Journal of Molecular Spectroscopy **227** 162–171 (2004).

[9] D. Robert and J. Bonamy. Short range force effects in semiclassical molecular line broadening calculations. Journal de Physique France **40** 923-943 (1979).

[10] Daniel Lisak, Joseph T. Hodges and Roman Ciuryło. Comparison of semiclassical line-shape models to rovibrational H_2O spectra measured by frequency-stabilized cavity ring-down spectroscopy. Physical Review A **73** 012507 (2006).

[11] Daniel Lisak, Joseph T. Hodges. Low-uncertainty H_2O line intensities for the 930 nm region. Journal of Molecular Spectroscopy **249** 6–13 (2008).

[12] David R. Thompson, D. Chris Benner, Linda R. Brown, David Crisp, V. Malathy Devi, Yibo Jiang *et al*. Atmospheric validation of high accuracy CO_2 absorption coefficients for the OCO-2 mission. Journal of Quantitative Spectroscopy and Radiative Transfer **113** 2265–2276 (2012).

[13] De Vizia MD, Rohart F, Castrillo A, Fasci E, Moretti L, Gianfrani L. Investigation on speed dependent effects in the near-IR spectrum of self-colliding $H_2{}^{18}O$ molecules. Physical Review A **83** 052506 (2011).

[14] Dennis L. Hartmann. Global Physical Climatology. Academic press 1994.

[15] F. Rohart, A. Ellendt, F. Kaghat and H. Mäder. Self and Polar Foreign Gas Line Broadening and Frequency Shifting of CH_3F: Effect of the Speed Dependence Observed by Millimeter-Wave Coherent Transients. Journal of Molecular Spectroscopy **185** 222-233 (1997).

[16] François Rohart, Heinrich Mäder, and Hans-Werner Nicolaisen. Speed dependence of rotational relaxation induced by foreign gas collisions: Studies on CH_3F by millimeter wave coherent transients. Journal of Chemical Physics **101** 6475-6486 (1994).

[17] Franz Schreier. Optimized implementations of rational approximations for the Voigt and complex error function. Journal of Quantitative Spectroscopy & Radiative Transfer **112** 1010-1025 (2011).

[18] G. Durry and G. Megie. Atmospheric CH_4 and H_2O monitoring with near-infrared InGaAs laser diodes by the SDLA, a balloonborne spectrometer for tropospheric and stratospheric in situ measurements. Applied optics **38** 7342–7354 (1999).

[19] G. Durry, V. Zeninari, B. Parvitte, T. Le barbu, F. Lefevre, J. Ovarlez, R.R. Gamache. Pressure-broadening coefficients and line strengths of H_2O near 1.39 mm: application to the in situ sensing of the middle atmosphere with balloonborne diode lasers. Journal of Quantitative Spectroscopy & Radiative Transfer **94** 387–403 (2005).

[20] G. Larcher, X. Landsheere, M. Schwell, H. Tran, Spectral shape parameters of pure CO_2 transitions near 1.6 mm by tunable diode laser spectroscopy, Journal of Quantitative Spectroscopy and Radiative Transfer **164** 82-88 (2015).

[21] H. Tran and J. M. Hartmann. An isolated line-shape model based on the Keilson and Storer function for velocity changes. I. Theoretical approaches. Journal of Chemical Physics **130** 094301 (2009).

[22] H. Tran, D. Bermejo, J.-L. Domenech, P. Joubert, R. R. Gamache, and J.-M. Hartmann. Collisional parameters of H_2O lines: Velocity effects on the line-shape. Journal of Quantitative Spectroscopy & Radiative Transfer **108** 126-145 (2007).

[23] H. Tran, J.-M. Hartmann, F. Chaussard, and M. Gupta. An isolated line-shape model based on the Keilson–Storer function for velocity changes. II. Molecular dynamics simulations and the Q(1) lines for pure H_2. Journal of Chemical Physics **131** 154303 (2009).

[24] H. Tran, N. H. Ngo, J.-M. Hartmann, R. R. Gamache, D. Mondelain *et al*. Velocity effects on the shape of pure H_2O isolated lines : Complementary tests of the partially correlated speed-dependent Keilson-Storer model. Journal of Chemical Physics **138** 034302 (2013).

[25] H. Tran, N.H. Ngo, J.-M. Hartmann. Efficient computations of some speed-dependent isolated line profiles. Journal of Quantitative Spectroscopy and Radiative Transfer **134**, 199-203 (2013).

[26] Hejie Li, Aamir Farooq, Jay B. Jeffries, Ronald K. Hanson. Diode laser measurements of temperature-dependent collisional-narrowing and broadening parameters of Ar-perturbed H_2O transitions at 1391.7 and 1397.8 nm. Journal of Quantitative Spectroscopy and Radiative Transfer **109** 132–143 (2008).

[27] Herbert M. Pickett. Effects of velocity averaging on the shape of absorption lines. Journal of Chemical Physics **73** 6090 (1980).

[28] Hui Su, William G. Read, Jonathan H. Jiang, Joe W. Waters, Dong L. Wu, and Eric J. Fetzer. Enhanced positive water vapor feedback associated with tropical deep convection: New evidence from Aura MLS. Geophysical Research Letter **33** L05709 (2006).

[29] J. Hansen, R. Ruedy, M. Sato, and K. Lo. Global surface temperature change. Reviews of Geophysics ***48*** *RG4004 (2010).*

[30] J. Humlicek. An efficient method for evaluation of the complex probability function: The Voigt function and its derivatives. Journal of Quantitative Spectroscopy & Radiative Transfer **21** 309-313 (1979).

[31] J. Humlicek. Optimized computation of the voigt and complex probability functions. Journal of Quantitative Spectroscopy & Radiative Transfer **27** 437-444 (1982).

[32] J. Keilson and J.E. Storrer. On Brownian motion, Boltzmanns equation, and the Forkker – Planck equation. Quarterly of Applied Mathematics **10** 243-253 (1952).

[33] J. M. Hartmann, C. Boulet, H. Tran, and M. T. Nguyen. Molecular dynamics simulations for CO_2 absorption spectra. I. Line broadening and the far wing of the ν_3 infrared band.. Journal of Chemical Physics **133** 144313 (2010).

[34] J. R. Pardo, J. Cernicharo, E. Lellouch, G. Paubert. Ground-Based measurements of middle atmospheric water vapor at 183 GHz. Journal of Geophysical Research 101 28723–28730 (1996).

[35] J. Tennyson, P. Bernath, A. Campargue, A. G. Csaszar, L. Daumont, R. R. Gamache, J. T. Hodges, D. Lisak, O. V. Naumenko, L. S. Rothman, H. Tran, N. F. Zobov, J. Buldyreva, C. Boone, M. D. De Vizia, L. Gianfrani, J.-M. Hartmann, R. McPheat, D. Weidmann, J. Murray, N. H. Ngo, O. L. Polyansky. Recommended isolated line profile for representing high-resolution spectroscopic transitions. P. Appl. Chem., 86, 1931-1943 (2014)

[36] J. Tennyson, P.F. Bernath, A. Campargue, et al. Recommended isolated line profile for representing high resolution spectroscopic transitions (IUPAC Technical Report). Pure and Applied Chemistry, **86** 0208 (2014)

[37] J. M. Hartmann, C. Boulet, and D. Robert. Collisional effects on molecular spectra. Laboratory experiments and models, consequences for applications, Elsevier, Amsterdam, 2008.

[38] Jung-Jung Tsou, John J. Olivero, Charles L. Croskey**.** Study of variability of mesospheric H_2O during spring 1984 by ground-based microwave radiometric observations. Journal of Geophysical Research **93** 5255–5266 **(**1988**).**

[39] Kendra L. Letchworth, D. Chris Benner. Rapid and accurate calculation of the Voigt function. Journal of Quantitative Spectroscopy & Radiative Transfer **107** 173-192 (2007).

[40] Louis Galatry. Simultaneous effect of Doppler and foreign gas broadening on spectral lines. Physical Review **122** 1218–1223 (1961).

[41] M. Kuntz. A new implementation of the Humlicek algorithm for the calculation of the Voigt profile function. Journal of Quantitative Spectroscopy & Radiative Transfer **57** 819-824 (1997).

[42] M. Milz, T. von Clarmann, H. Fischer, N. Glatthor, U. Grabowski, M. Höpfner et al. Water vapor distributions measured with the Michelson Interferometer for Passive Atmospheric Sounding on board Envisat (MIPAS/Envisat). Geophysical Research Letter **110** D24307 (2005).

[43] M. Nelkin and A. Ghatak. Simple Binary Collision Model for Van Hove's $G_s(r, t)$. Physical Review **135** A4-A9 (1964).

[44] M. Schneider and F. Hase. Ground-based FTIR water vapour profile analyses. Atmospheric Measurement Techniques **2** 609-619 (2009).

[45] Milton Abramowitz, Irene A.Stegun. Handbook of Mathematical Functions with Formulas, Graphs, and Mathematical Tables. New York: Dover Publications (1972).

[46] Muriel Lepère, Annie Henry, Alain Valentin and Claude Camy-Peyret. Diode-Laser Spectroscopy: Line Profiles of H_2O in the Region of 1.39 μm. Journal of Molecular Spectroscopy **208** 25–31 (2001).

[47] N. H. Ngo, D. Lisak, H. Tran, J.-M. Hartmann. An isolated line-shape model to go beyond the Voigt profile in spectroscopic databases and radiative transfer codes. Journal of Quantitative Spectroscopy and Radiative Transfer **129**, 89-100 (2013).

[48] N. H. Ngo, H. Tran and R. R. Gamache. A pure H_2O isolated line-shape model based on classical molecular dynamics simulations of velocity changes and semi-classical calculations of speed-dependent collisional parameters. Journal of Chemical Physics **136** 154310 (2012).

[49] N. H. Ngo, H. Tran, R. R. Gamache, D. Bermejo, and J.-L. Domenech. Influence of velocity effects on the shape of N_2 (and air) broadened H_2O lines revisited with classical molecular dynamics simulations. Journal of Chemical Physics **137** 064302 (2012).

[50] N. H. Ngo, H. Tran, R. R. Gamache, J. M. Hartmann. Pressure effects on water vapor lines : beyond the Voigt profile. Royal Society of Chemistry journal **370** 2495-2508 (2012).

[51] N. H. Ngo, N. Ibrahim, X. Landsheere, H. Tran, P. Chelin, M. Schwell and J. M. Hartmann. Intensities and shapes of H_2O lines in the near-infrared by tunable diode laser spectroscopy. Journal of Quantitative Spectroscopy and Radiative Transfer **113** 870-877 (2012).

[52] J. S. Wilzewski, M. Birk, J. Loos, and G. Wagner, J. Quant. Spectrosc. Radiat. Transfer **206**, 296–305 (2018).

[53] N. Jacquinet-Husson, L. Crepeau et al. The 2009 edition of the GEISA spectroscopic database Journal of Quantitative Spectroscopy and Radiative Transfer **112** 2395-2445 (2011).

[54] Paul R. Berman. Speed-dependent collisional width and shift parameters in spectral profiles. Journal of Quantitative Spectroscopy and Radiative Transfer **12** 1331-1342 (1972).

[55] R.H. Dicke. The effect of collisions upon the Doppler width of spectral lines. Physical Review **89** 472–473 (1953).

[56] V. M. Devi, D. C. Benner, K. Sung, L. R. Brown, T. J. Crawford, C. E. Miller, B. J. Drouin, V. H. Payne, S. Yu, M. A. H. Smith, A. W. Mantz, and R. R. Gamache, J. Quant. Spectrosc. Radiat. Transfer **177**, 117 (2016).

[57] D. C. Benner, V. M. Devi, K. Sung, L. R. Brown, C. E. Miller, V. H. Payne, B. J. Drouin, S. Yu, T. J. Crawford, A. W. Mantz, M. A. H. Smith, and R. R. Gamache, J. Mol. Spectrosc. **326**, 21 (2016).

[58] M. Ghysels, Q. Liu, A. J. Fleisher, and J. T. Hodges, Appl. Phys. B: Lasers Opt. **123**, 124 (2017).

[59] Rothman LS, Gordon IE et al. The HITRAN 2008 molecular spectroscopic database. Journal of Quantitative Spectroscopy and Radiative Transfer **110** 533-572 (2009).

[60] Rothman LS, Gordon IE et al. The HITRAN 2012 molecular spectroscopic database. Journal of Quantitative Spectroscopy and Radiative Transfer **130** 4-50 (2013).

[61] W. Voigt. Über das gesetz intensitätsverteilung innerhalb der linien eines gasspektrams. Sitzber. Bayr Akad. München Ber. 603-620 (1912).

[62] R.J. Wells. Rapid approximation to the Voigt/Faddeeva function and its derivatives. Journal of Quantitative Spectroscopy & Radiative Transfer **62** 29-48 (1999).

[63] Rautian SG. Sobel'man II. The effect of collisions on the Doppler broadening of spectral lines. Soviet Physics Uspekhi **9** 701–716 (1967).

[64] Ray Nassar, Peter F. Bernath, Chris D. Boone, Gloria L. Manney, Sean D. McLeod, Curtis P. Rinsland, Randall Skelton, and Kaley A. Walker. Stratospheric abundances of water and methane based on ACE-FTS measurements. Geophysical Research Letter **32** L15S04 (2005).

[65] Long DA, Wojtewicz S, Miller CE, Hodges JT. Frequency-agile, rapid scanning cavity ring-down spectrosocpy (FARS-CRDS) measurements of the (30012)←(00001) mear-infrared carbon dioxide band. J Quant Spectrosc Rad Transf 2015;161:35–40.

[66] Benner DC, Devi VM, Sung K, et al. Line parameters including temperature dependences of air- and self-broadened line shapes of 12C16O2: 2.06-μm region. J Mol Spectrosc 2016;326:31–47.

[67] N. H. Ngo, D. Lisak, H. Tran, and J. M. Hartmann, J. Quant. Spectrosc. Radiat. Transfer **134**, 105 (2014).

[68] Ghysels M, Liu Q, Fleisher AJ, Hodges JT. A variable-temperature cavity ring– down spectrometer with application to line shape analysis of CO2 spectra in the 1600 nm region. Appl Phys B 2017;123-124:1–13.

[69] Wilzewski JS, Birk M, Loos J, Wagner G. Temperature-dependence laws of absorption line shape parameters of the CO2 ν3 band. J Quant Spectrosc Rad Transf 2018;206:296–305.

[70] Nguyen HT, Ngo NH, Tran H. Prediction of line shape parameters and their temperature dependences for CO2-N2 using molecular dynamics simulations. J Chem Phys 2018;149:224301.

[71] G. Larcher, H. Tran, M. Schwell, P. Chelin, X. Landsheere, J. M. Hartmann, and S. M. Hu, J. Chem. Phys. **140**, 084308 (2014).

[72] J.-M. Hartmann, H. Tran, N. H. Ngo, X. Landsheere, P. Chelin, Y. Lu, A.- W. Liu, S.-M. Hu, L. Gianfrani, G. Casa, A. Castrillo, M. Lepere, Q. Deli ` ere, ` M. Dhyne, and L. Fissiaux, Phys. Rev. A **87**, 013403 (2013).

[73] J. Bouanich, J. Quant. Spectrosc. Radiat. Transfer **47**, 243 (1992).

[74] Murthy CS, O'Shea SF, McDonald IR. Electrostatic interactions in molecular crystals lattice dynamics of solid nitrogen and carbon dioxide. Mol Phys 1983;50:531–41.

[75] Rosenkranz PK. Shape of the 5 mm oxygen band in the atmosphere. IEEE Trans Antennas Propag 1975;23:498–506.

[76] N. H. Ngo, D. Lisak, H. Tran, and J. M. Hartmann, J. Quant. Spectrosc. Radiat. Transfer **129**, 89 (2013).

[77] Devi VM, Benner DC, Miller CE, Predoi-Cross A. Lorentz half-width, pressure-induced shift and speed-dependent coefficients in oxygen-broadened CO2 bands at 6227 and 6348 cm-1 using a constrained multispectrum analysis. J Quant Spectrosc Radiat Transf 2010;111:2355–69.

[78] Hikida T, Yamada KMT. N2- and O2-broadening of CO2 for the (300 1)III ← (0000) band at 6231 cm-1. J Mol Spectrosc 2006;239:154–9.

[79] Gordon IE, Rothman LS, Hill C, Kochanov RV, Tan Y, Bernath PF, Birk M, Boudon CampargueA, Chance KV, Drouin BJ, Flaud JM, Gamache RR, Hodges JT, Jacquemart D, Perevalov VI, Perrin A, Shine KP, Smith MAH, Tennyson J, Toon GC, Tran H, Tyuterev VG, Barbe A, Császár AG, Devi VM, Furtenbacher T, Harrison JJ, Hartmann J-M, Jolly A, Johnson TJ, Karman T, Kleiner I, Kyuberis AA, Loos J, Lyulin OM, Massie ST, Mikhailenko SN, Moazzen-Ahmadi N, Müller HSP, Naumenko OV, Nikitin AV, Polyansky OL, Rey M, Rotger M, Sharpe SW, Sung K, Starikova E, Tashkun SA, Vander Auwera J, Wagner G, Wilzewski J, Wcisło P, Yu S, Zak EJ. The HITRAN2016 molecular spectroscopic database. J Quant Spectrosc Radiat Transf 2017;203:3–69. doi:10.1016/j.jqsrt. 2017.06.038.

[80] Lamouroux J, Régalia L, Thomas X, Vander Auwera J, Gamache RR, Hartmann JM. CO2 line-mixing database and software update and its tests in the 2.1 μm and 4.3 μm regions. J Quant Spectrosc Radiat Transfer 2015;151:88–96.

[81] Predoi-Cross A, Liu W, Holladay C, Unni AV, Schofield I, McKellar ARW, Hurtmans D. Line profile study of transitions in the 30012←00001 and 30013←00001 bands of carbon dioxide perturbed by air. J Mol Spectrosc 2007;

[82] M. P. Allen and D. J. Tildesley, *Computer Simulations of Liquids* (Oxford University Press, Oxford, 1987).

[83] J. E. Hirschfelder, C. F. Curtiss, and R. B. Bird, *Molecular Theory of Gases and Liquids* (Wiley, New York, 1954).

[84] N. H. Ngo and J. M. Hartmann, J. Quant. Spectrosc. Radiat. Transfer **203**, 334 (2017).

[85] M. Nelkin and A. Ghatak, Phys. Rev. **135**, A4 (1964).

[86] S. G. Rautian and I. L. Sobel'man, Sov. Phys. Uspekhi **9**, 701 (1967).

[87] F. Rohart, H. Mader, and H. Nicolaisen, J. Chem. Phys. **101**, 6475 (1994).

[88] D. Lisak, D. K. Havey, and J. T. Hodges, Phys. Rev. A **79**, 052507 (2009).

[89] Tran DD, Sironneau VT, Hodges JT, Armante R, Cuesta J, Tran H. Prediction of high-order line-shape parameters for air-broadened O2 lines using requantized classical molecular dynamics simulations and comparison with measurements. J Quant Spectrosc Rad Transf 2019;222 223:108–14.

[90] Lamouroux J, Sironneau V, Hodges JT, Hartmann JM. Isolated line shapes of molecular oxygen: requantized classical molecular dynamics calculations versus measurements. Phys Rev A 2014;89:042504. doi:10.1103/PhysRevA.89. 042504.

[91] Rohart F, Ellendt A, Kaghat K, Mäder H. Self and polar foreign gas line broadening and frequency shifting of CH3F: effect of the speed dependence observed by millimeter-wave coherent transients. J Mol Spectrosc 1997;185:222–33.

[92] Rohart F, Colmont JM, Wlodarczak G, Bouanich JP. N_2- and O_2-broadening coefficients and profiles for millimeter lines of $^{14}N_2O$. J Mol Spectrosc 2003;222:159-171.

[93] H. Tran, G. Li, V. Ebert, and J.-M. Hartmann, J. Chem. Phys. **146**, (2017).

[94] Ngo NH, Lin H, Hodges JT, Tran H. Spectral shapes of rovibrational lines of CO broadened by He, Ar, Kr and SF_6: A test case of the Hartmann-Tran profile. J Quant Spectrosc Rad Transfer 2017;203:325-333.

[95] Hartmann JM, Tran H, Armante R, Boulet C, Campargue A, Ciurylo R, Forget F, Gianfrani L, Gordon I, Guerlet S, Gustafsson M, Hodges J, Kassi S, Lisak D, Thibault F, Toon GC. Recent advances in collisional effects on spectra of molecular gases and their pratical consequences. J Quant Spectrosc Radiat Transfer 2018;213:178-227.

[96] Thinh Q. Bui, David A. Long, Agata Cygan, Vincent T. Sironneau, Daniel W. Hogan, Priyanka M. Rupasinghe, Roman Ciuryło, Daniel Lisak, and Mitchio Okumura. Observations of Dicke narrowing and speed dependence in air-broadened CO2 lineshapes near 2.06 µm. *The Journal of Chemical Physics 141, 174301 (2014); doi: 10.1063/1.4900502*

[97] Loos J, Birk M, Wagner G. Pressure broadening, -shift, speed dependence and line mixing in the ν_3 rovibational band of N_2O. J Quant Spectrosc Transf 2015;151:300-9.